Eur. Phys. J. C (2020) 80:189
https://doi.org/10.1140/epjc/s10052-020-7739-7

THE EUROPEAN PHYSICAL JOURNAL C

Regular Article - Experimental Physics

Search for direct pair production of supersymmetric partners to the τ lepton in proton–proton collisions at $\sqrt{s} = 13$ TeV

CMS Collaboration*

CERN, 1211 Geneva 23, Switzerland

Received: 30 July 2019 / Accepted: 11 February 2020

Abstract A search is presented for τ slepton pairs produced in proton–proton collisions at a center-of-mass energy of 13 TeV. The search is carried out in events containing two τ leptons in the final state, on the assumption that each τ slepton decays primarily to a τ lepton and a neutralino. Events are considered in which each τ lepton decays to one or more hadrons and a neutrino, or in which one of the τ leptons decays instead to an electron or a muon and two neutrinos. The data, collected with the CMS detector in 2016 and 2017, correspond to an integrated luminosity of 77.2 fb^{-1}. The observed data are consistent with the standard model background expectation. The results are used to set 95% confidence level upper limits on the cross section for τ slepton pair production in various models for τ slepton masses between 90 and 200 GeV and neutralino masses of 1, 10, and 20 GeV. In the case of purely left-handed τ slepton production and decay to a τ lepton and a neutralino with a mass of 1 GeV, the strongest limit is obtained for a τ slepton mass of 125 GeV at a factor of 1.14 larger than the theoretical cross section.

1 Introduction

Supersymmetry (SUSY) [1–8] is a possible extension of the standard model (SM) of particle physics, characterized by the presence of superpartners for SM particles. The superpartners have the same quantum numbers as their SM counterparts, except for the spin, which differs by half a unit. One appealing feature of SUSY is that the cancellation of quadratic divergences in quantum corrections to the Higgs boson mass from SM particles and their superpartners could resolve the fine tuning problem [9–12]. Another feature is that the lightest supersymmetric particle (LSP) is stable in SUSY models with R-parity conservation [13], and could be a dark matter (DM) candidate [14–16].

The hypothetical superpartner of the τ lepton, the τ slepton ($\tilde{\tau}$), is the focus of the search reported in this paper. Supersymmetric models where a light $\tilde{\tau}$ is the next-to-lightest supersymmetric particle are well motivated in early universe $\tilde{\tau}$-neutralino coannihilation models that can accommodate the observed DM relic density [17–22]. The existence of a light $\tilde{\tau}$ would enhance the rate of production of final states with τ leptons in collider experiments [23,24].

In this analysis, we study the simplified model [25–27] of direct $\tilde{\tau}$ pair production shown in Fig. 1. We assume that the $\tilde{\tau}$ decays to a τ lepton and $\tilde{\chi}_1^0$, the lightest neutralino, which is the LSP in this model. The search is challenging because of the extremely small production cross section expected for this signal, as well as the large backgrounds. The most sensitive previous searches for direct $\tilde{\tau}$ pair production were performed at the CERN LEP collider [28–31], excluding $\tilde{\tau}$ masses at 95% confidence level (CL) up to ≈90 GeV for neutralino masses up to 80 GeV in some models. At the LHC, the ATLAS [32,33] and CMS [34] Collaborations have also performed searches for direct $\tilde{\tau}$ pair production using 8 TeV data, and the CMS Collaboration has reported a search for direct $\tilde{\tau}$ pair production in an initial sample of 35.9 fb^{-1} at 13 TeV collected in 2016 [35]. This paper presents a significant improvement in search sensitivity, which was limited by the small signal production rates, through the incorporation of improved analysis techniques and the inclusion of the data collected in 2017. The data used correspond to a total integrated luminosity of 77.2 fb^{-1}.

Events with two τ leptons are used. We consider both hadronic and leptonic decay modes of the τ lepton, in which it decays to one or more hadrons and a neutrino, or to an electron or muon and two neutrinos, respectively. Independent analyses are carried out in the final states with two hadronically decaying τ leptons ($\tau_h\tau_h$) and with one τ_h and an electron or a muon ($\ell\tau_h$, where ℓ = e or μ). The presence of missing transverse momentum, which can originate from stable neutralinos as well as neutrinos from τ lepton decays, provides an important source of discriminating power between signal and background.

*e-mail: cms-publication-committee-chair@cern.ch (corresponding author)

Published online: 02 March 2020

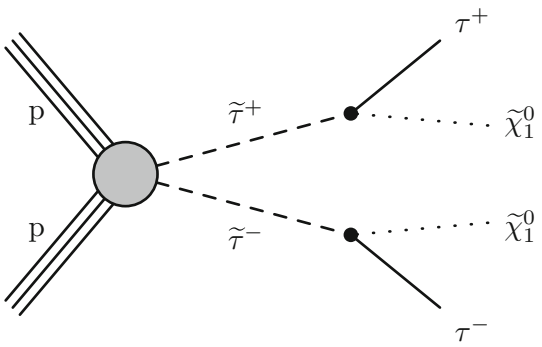

Fig. 1 Diagram for direct $\tilde{\tau}$ pair production, followed by decay of each $\tilde{\tau}$ to a τ lepton and a $\tilde{\chi}_1^0$

We have introduced several improvements with respect to the analysis presented in Ref. [35] that are applied to both 2016 and 2017 data. We make use of dedicated machine learning techniques to enhance the search sensitivity. These include the incorporation of an improved τ_h selection method that makes use of a deep neural network (DNN) for the $\tau_h\tau_h$ analysis, and of a boosted decision tree (BDT) for event selection in the $\ell\tau_h$ analyses. Improvements have also been made to the background-estimation techniques and to the search region (SR) definitions. The incorporation of these enhancements is expected to improve the search sensitivity by up to 50%, where the figure of merit considered is the 95% CL upper limit on the cross section for $\tilde{\tau}$ pair production obtained with the data collected in 2016. The improvement is less significant than expected, since it is found that the estimated signal acceptance is reduced when the fast detector simulation that was previously used to model signal events is replaced in this search with the more realistic, full GEANT4-based detector simulation [36]. Differences in the signal acceptance for the fast and more accurate full detector simulations are mainly caused by differences in the reconstructed τ_h visible transverse momentum (p_T), which is found to have larger values in the case of the fast simulation.

We consider the superpartners of both left- and right-handed τ leptons, $\tilde{\tau}_L$ and $\tilde{\tau}_R$. The cross section for $\tilde{\tau}_L$ pair production is expected to be about a factor of three larger than for $\tilde{\tau}_R$ pairs [37]. The experimental acceptance is also expected to be different for left- and right-handed assignments because of the differences in the polarization of the τ leptons produced in $\tilde{\tau}_L$ and $\tilde{\tau}_R$ decays. The decay products of hadronically and leptonically decaying τ leptons originating from $\tilde{\tau}_R$ decays are predicted to have larger and smaller p_T, respectively, than those originating from $\tilde{\tau}_L$ decays. Two simplified models are studied for direct $\tilde{\tau}$ pair production. One model involves production of only $\tilde{\tau}_L$ pairs and the other is for the degenerate case in which both $\tilde{\tau}_L$ and $\tilde{\tau}_R$ pairs are produced. No mixing is introduced between left- and right-handed states. We study models with $\tilde{\tau}$ masses ranging from 90 to 200 GeV. The LEP limits [28–31] place strong constraints on the allowed values of the $\tilde{\tau}$ mass below this range, while the search sensitivity for $\tilde{\tau}$ masses above this range is low as a result of the decrease in production cross section with increased mass. We also consider different assumptions for the $\tilde{\chi}_1^0$ mass, namely 1, 10, and 20 GeV. The search sensitivity decreases when the mass difference between the $\tilde{\tau}$ and $\tilde{\chi}_1^0$ becomes small, since the visible decay products in such cases have lower momentum, resulting in a loss of experimental acceptance for such signals.

2 The CMS detector

The central feature of the CMS apparatus is a superconducting solenoid of 6 m internal diameter, providing a magnetic field of 3.8 T. A silicon pixel and strip tracker, a lead tungstate crystal electromagnetic calorimeter (ECAL), and a brass and scintillator hadron calorimeter, each composed of a barrel and two endcap sections, reside within the solenoid volume. Forward calorimeters extend the pseudorapidity (η) coverage provided by the barrel and endcap detectors. Muons are detected in gas-ionization chambers embedded in the steel flux-return yoke outside the solenoid. Events of interest are selected using a two-tiered trigger system [38]. The first level, composed of custom hardware processors, uses information from the calorimeters and muon detectors to select events at a rate of around 100 kHz within a time interval of less than 4 μs. The second level, known as the high-level trigger, consists of a farm of processors running a version of the full event reconstruction software optimized for fast processing, which reduces the event rate to about 1 kHz before data storage. A more detailed description of the CMS detector, together with definitions of the coordinate system and kinematic variables, can be found in Ref. [39].

3 Event reconstruction and simulation

The event reconstruction uses a particle-flow (PF) algorithm [40] that combines information from the tracker, calorimeter, and muon systems to identify charged and neutral hadrons, photons, electrons, and muons in an event. The missing transverse momentum vector, $\vec{p}_T^{\,\text{miss}}$, is computed as the negative of the vector sum of the p_T of all PF candidates reconstructed in an event, and its magnitude p_T^{miss} is used in the search as a discriminator between signal and SM background. Events selected for the search are required to pass filters [41] designed to remove detector- and beam-related backgrounds, and must have at least one reconstructed vertex. Usually, more than one such vertex is reconstructed because of pileup, i.e., multiple proton–proton (pp) collisions within the same or neighboring bunch crossings. The mean num-

ber of interactions per bunch crossing was 27 in 2016, and increased to 37 in 2017, assuming a total inelastic pp cross section of 80 mb. The reconstructed vertex with the largest value in summed object p_{T}^2 is selected to be the primary pp interaction vertex (PV). These objects are defined by tracks associated with a given vertex that are clustered using a jet finding algorithm [42,43], and a more restricted form of the vector missing transverse momentum that is calculated from these track-based jets.

Charged particles that originate from the PV, photons, and neutral hadrons are clustered into jets using the anti-k_{T} algorithm [42] with a distance parameter of 0.4, as implemented in the FastJet package [43]. The jet energies are corrected to account for the contribution from pileup interactions and to compensate for variations in the detector response [43,44]. To mitigate issues related to noise in the ECAL endcaps that led to significantly worse modeling of the $p_{\mathrm{T}}^{\mathrm{miss}}$ distribution, particularly for events with large values of $p_{\mathrm{T}}^{\mathrm{miss}}$ in 2017 data, PF candidates that are clustered in jets in $2.65 < |\eta| < 3.14$ with uncorrected $p_{\mathrm{T}} < 50\,\mathrm{GeV}$ are not used in the calculation of $\vec{p}_{\mathrm{T}}^{\,\mathrm{miss}}$ in 2017 data and simulation. Disagreements between the $p_{\mathrm{T}}^{\mathrm{miss}}$ distributions in data and simulation ranging up to >100% for $50 < p_{\mathrm{T}}^{\mathrm{miss}} < 170\,\mathrm{GeV}$ in DY+jets events, in which large values of $p_{\mathrm{T}}^{\mathrm{miss}}$ arise mainly from mismeasurements, are reduced by this modification of the $\vec{p}_{\mathrm{T}}^{\,\mathrm{miss}}$ calculation. The modified $p_{\mathrm{T}}^{\mathrm{miss}}$ distributions in simulated events and data agree within uncertainties.

Jets in the search are required to have their axes within the tracker volume of $|\eta| < 2.4$. For the $\tau_{\mathrm{h}}\tau_{\mathrm{h}}$ analysis, we use jets with $p_{\mathrm{T}} > 30\,\mathrm{GeV}$, while for the $\ell\tau_{\mathrm{h}}$ analyses, we veto events containing jets with $p_{\mathrm{T}} > 20\,\mathrm{GeV}$ to provide efficient background rejection. Jets are required to be separated in η and azimuthal angle (ϕ) by $\Delta R \equiv \sqrt{(\Delta\eta)^2 + (\Delta\phi)^2} > 0.4$ from electron, muon, or τ_{h} candidates in order to minimize double counting of objects. Jets originating from the hadronization of b quarks are "tagged" in the $\tau_{\mathrm{h}}\tau_{\mathrm{h}}$ analysis through the DNN-based combined secondary vertex algorithm (DeepCSV) [45] to reject events with b quark jets that are likely to originate from backgrounds with top quarks. The efficiency for tagging b quarks originating from top quark decays is about 84%, while the misidentification rates for jets from charm quarks, and from light quarks or gluons, are about 41 and 11%, respectively. In the $\ell\tau_{\mathrm{h}}$ analyses, the CSVv2 tagger [45] is used to identify b quark jets for the selection of background-enriched control regions (CRs). The working point that is used corresponds to an efficiency of 63% and misidentification rates of 12 and 0.9% for jets from charm quarks and light quarks or gluons, respectively.

Electron candidates are reconstructed by first matching reconstructed tracks to clusters of energy deposited in the ECAL. Selections based on the spatial distribution of the shower, track–cluster matching criteria, and consistency between the cluster energy and the track momentum are then used in the identification of electron candidates [46]. Muon candidates are reconstructed by requiring reconstructed tracks in the muon detector to be matched to the tracks found in the inner tracker [47]. We require the origin of electron and muon candidates to be consistent with the PV. Restrictions are imposed on the magnitude of the impact parameters of their tracks relative to the PV in the transverse plane (d_{xy}), and on the longitudinal displacement (d_z) of the point of closest approach. To ensure that electron or muon candidates are isolated from jet activity, we define a relative isolation quantity (I_{rel}) as the ratio of the scalar p_{T} sum of hadron and photon PF candidates, in an η-ϕ cone of radius 0.3 or 0.4 around the candidate electron or muon, to the candidate p_{T}, requiring it to be below an upper bound appropriate for the selection. The quantity I_{rel} is adjusted to account for the contributions of particles originating from pileup interactions. The electron and muon selection criteria applied in the analysis are the same as those described in Ref. [35].

The τ_{h} candidates are reconstructed using the CMS hadrons-plus-strips algorithm [48]. The constituents of the reconstructed jets are used to identify individual τ lepton decay modes with one charged hadron and up to two neutral pions, or three charged hadrons. The τ_{h} candidate momentum is determined from the reconstructed visible τ lepton decay products. The presence of extra particles within the jet that are incompatible with the reconstructed decay mode is used as a criterion to discriminate jets from τ_{h} decays. A multivariate-analysis (MVA) based discriminant [48], which contains isolation as well as lifetime information, is used to suppress the rate for quark and gluon jets to be misidentified as τ_{h} candidates. We employ a relaxed ("very loose") working point of this discriminant as a preselection requirement for the τ_{h} candidates selected in the $\tau_{\mathrm{h}}\tau_{\mathrm{h}}$ analysis, as well as in the extrapolation used to estimate the contributions of events to the background in which quark or gluon jets are misidentified as τ_{h} candidates. This working point corresponds to an efficiency of ≈70% for a genuine τ_{h}, and a misidentification rate of ≈1% for quark or gluon jets. A DNN is used to improve the discrimination of signal τ_{h} candidates from background, as discussed in more detail below. Two working points are used in the $\ell\tau_{\mathrm{h}}$ analysis: a "very tight" working point for selecting signal τ_{h} candidates that provides stringent background rejection, and a "loose" working point for the extrapolation procedure to estimate the misidentified τ_{h} background that provides higher efficiency and less background rejection. These working points, respectively, typically have efficiencies close to 45 and 67% for a genuine τ_{h}, with misidentification rates of ≈0.2 and 1% for quark or gluon jets. Electrons and muons misidentified as a τ_{h} are suppressed via criteria specifically developed for this purpose that are based on the consistency of information from the tracker, calorimeters, and muon detectors [48].

The dominant background in the $\tau_h\tau_h$ final state originates from misidentification of jets as τ_h candidates, mainly in SM events exclusively comprising jets produced through the strong interaction of quantum chromodynamics (QCD). These are referred to as QCD multijet events in what follows. To further improve the suppression of this background while retaining high signal efficiency, we have pursued a new approach for τ_h isolation in the $\tau_h\tau_h$ analysis that is based upon the application of a DNN that is fed information about the properties of PF candidates within an isolation cone with $\Delta R < 0.5$ around the τ_h candidate. We refer to this as "Deep Particle Flow" (DeepPF) isolation. Charged PF candidates consistent with having originated from the PV, photon candidates, and neutral hadron candidates with $p_T > 0.5$, 1, and 1.25 GeV, respectively, provide the inputs to the DeepPF algorithm. The list of observables incorporated for each PF candidate includes its p_T relative to the τ_h jet, ΔR between the candidate and τ_h, particle type, track quality information, and d_{xy}, d_z and their uncertainties, $\sigma(d_{xy})$ and $\sigma(d_z)$. A convolutional DNN [49] is trained with simulated signal and background events. Signal τ_h candidates are those that are matched to generator-level τ leptons from a mixture of processes that give rise to genuine τ leptons. Background candidates that fail the matching are taken from simulated W+jets and QCD multijet events. The DeepPF discriminator value is obtained by averaging the DNN output with the nominal MVA-based discriminant described above. The working point for DeepPF isolation is chosen to maintain a constant efficiency of ≈50%, 56%, and 56% as a function of p_T for the three respective τ_h decay modes: one charged hadron, one charged hadron with neutral pions, and three charged hadrons. Since the τ_h candidate p_T distribution in signal events depends on the $\widetilde{\tau}$ and $\widetilde{\chi}_1^0$ masses, this choice of discriminator and working points allows us to maintain high efficiency for $\widetilde{\tau}$ pair production signals under a large range of mass hypotheses. The overall misidentification rate for jets not originating from τ leptons ranges from 0.15% to 0.4% depending on p_T and decay mode.

Significant contributions to the SM background originate from Drell–Yan+jets (DY+jets), W+jets, $t\bar{t}$, and diboson processes, as well as from QCD multijet events, where DY corresponds to processes such as $q\bar{q} \to \ell^+\ell^-$. Smaller contributions arise from single top quark production and rare SM processes, such as triboson and Higgs boson production, and top quark pair production in association with vector bosons. We rely on a combination of measurements in data CRs and Monte Carlo (MC) simulation to estimate contributions of each source of background. The MC simulation is also used to model the signal.

The MadGraph5_aMC@NLO version 2.3.3 and 2.4.2 event generators [50] are used at leading order (LO) precision to generate simulated W+jets and DY+jets events with up to 4 additional partons for the analysis of 2016 and 2017 data, respectively. Exclusive event samples binned in jet multiplicity are used to enhance the statistical power of the simulation at higher values of jet multiplicity that are relevant to the phase space probed by this search. Production of top quark pairs, diboson and triboson events, and rare SM processes, such as single top quarks or top quark pairs associated with bosons, are generated at next-to-leading order (NLO) precision with MadGraph5_aMC@NLO and powhegv2 [51–54]. Showering and hadronization of partons are carried out using the pythia 8.205 and 8.230 packages [55] for the 2016 and 2017 analyses, respectively, while a detailed simulation of the CMS detector is based on the Geant4 [36] package. Finally, uncertainties in renormalization and factorization scale, and parton distribution functions (PDFs) have been obtained using the SysCalc package [56]. Models of direct $\widetilde{\tau}$ pair production are generated with MadGraph5_aMC@NLO at LO precision up to the production of τ leptons, with their decay modeled by pythia 8.212 and 8.230 for the analysis of 2016 and 2017 data, respectively. The CUETP8M1 [57] (CUETP8M2T4 [58] for $t\bar{t}$) and CP5 [59] underlying-event tunes are used with pythia for the 2016 and 2017 analyses, respectively. The 2016 analysis uses the NNPDF3.0LO [60] set of PDFs in generating W+jets, DY+jets, and signal events, while the NNPDF3.0NLO PDFs are used for other processes. The NNPDF3.1NLO PDFs are used for all simulated events in the 2017 analysis.

Simulated events are reweighted to match the pileup profile observed in data. Differences between data and simulation in electron, muon, and τ_h identification and isolation efficiencies, jet, electron, muon, and τ_h energy scales, and b tagging efficiency are taken into account by applying scale factors to the simulation. We improve the modeling of initial-state radiation (ISR) in simulated signal events by reweighting the p_T^{ISR} distribution, where p_T^{ISR} corresponds to the total transverse momentum of the system of SUSY particles. This reweighting procedure is based on studies of the p_T of Z bosons [61]. The signal production cross sections are calculated at NLO using next-to-leading logarithmic (NLL) soft-gluon resummations [37]. The most precise calculated cross sections available are used to normalize the simulated SM background samples, often corresponding to next-to-next-to-leading order accuracy.

4 Event selection

The search strategy in the $\tau_h\tau_h$ final state relies on a cut-and-count analysis based on the SRs described below in Sect. 4.1, while for the $\ell\tau_h$ final states we make use of BDTs to discriminate between signal and background as described in Sect. 4.2. The data used in this search are selected through triggers that require the presence of isolated electrons, muons, τ_h candidates, or p_T^{miss}. The data used for

the $\tau_h\tau_h$ analysis are collected with two sets of triggers. Events with $p_T^{miss} < 200$ GeV are selected using a trigger that requires the presence of two τ_h candidates, each with $p_T >$ 35 and >40 GeV in 2016 and 2017 data, respectively. We gain up to 7% additional signal efficiency for events with $p_T^{miss} >$ 200 GeV with the help of a trigger that requires the presence of substantial p_T^{miss}, with a threshold varying between 100 and 140 GeV during the 2016 and 2017 data-taking periods. For the $e\tau_h$ final state, the trigger relies on the presence of an isolated electron satisfying stringent identification criteria and passing $p_T > 25$ or >35 GeV in 2016 and 2017 data, respectively. For the $\mu\tau_h$ final state, the trigger is based on the presence of an isolated muon with $p_T > 24$ and >27 GeV in 2016 and 2017 data, respectively. Trigger efficiencies are measured in data and simulation. In addition to corrections mentioned in Sect. 3, we apply scale factors to the simulation to account for any discrepancies in trigger efficiency with data. These scale factors are parameterized in the p_T and η of the reconstructed electron, muon, or τ_h candidates, or the reconstructed p_T^{miss} for events selected using p_T^{miss} triggers.

4.1 Event selection and search regions in the $\tau_h\tau_h$ final state

Beyond the trigger selection, the baseline event selection for the $\tau_h\tau_h$ analysis requires the presence of exactly two isolated τ_h candidates of opposite charge, satisfying the DeepPF selection described in Sect. 3, with $|\eta| < 2.3$ and $p_T > 40$ and >45 GeV in the 2016 and 2017 analysis, respectively, as well as no additional τ_h candidates with $p_T > 30$ GeV satisfying the very loose working point of the MVA-based discriminant. We veto events with additional electrons or muons with $p_T > 20$ GeV and $|\eta| < 2.5$ or < 2.4 for electrons and muons, respectively, and reject any events with a b-tagged jet to suppress top quark backgrounds. A requirement of $|\Delta\phi(\tau_h^{(1)}, \tau_h^{(2)})| > 1.5$ helps to suppress the DY+jets background, while retaining high signal efficiency. Finally, we require $p_T^{miss} > 50$ GeV to suppress the QCD multijet background.

The removal of low-p_T jets in the forward ECAL region from the $\vec{p}_T^{miss}$ calculation in 2017 (see Sect. 3) causes the background originating from DY+jets and other sources to increase in the SRs, since events with low-p_T jet activity in that region are assigned larger values of reconstructed p_T^{miss}. We recover some of the corresponding loss in sensitivity in the 2017 analysis by placing an upper bound of 50 GeV on the scalar p_T sum of low-p_T jets excluded from the $\vec{p}_T^{miss}$ calculation (H_T^{low}). This restriction reduces the impact of background events with significant low-p_T jet activity in the forward region, for which the p_T^{miss} would be overestimated. To ensure that the efficiency of this requirement is correctly estimated in simulation, a $Z \to \mu^+\mu^-$ CR is used to extract correction factors for the H_T^{low} distribution in simulation that account for discrepancies with the distribution observed in data. The correction factors range from 0.8 for $H_T^{low} < 10$ GeV to 1.4 for $H_T^{low} > 60$ GeV. In addition, to avoid effects related to jet mismeasurement that can contribute to spurious p_T^{miss}, we require the $\vec{p}_T^{miss}$ to have a minimum separation of 0.25 in $|\Delta\phi|$ from jets with $p_T > 30$ GeV and $|\eta| < 2.4$, as well as from those with uncorrected $p_T > 50$ GeV in the region $2.4 < |\eta| < 3.14$.

Events satisfying the baseline selection criteria are subdivided into exclusive SRs using several discriminants. To improve the discrimination of signal from SM background, we take advantage of the expected presence of two $\tilde{\chi}_1^0$ in the final state of signal events and their contribution to p_T^{miss}. Their presence skews the correlations between $\vec{p}_T^{miss}$ and the reconstructed leptons to be different from background processes, even for those backgrounds with genuine p_T^{miss}. These differences can be exploited by mass observables calculated from the reconstructed lepton transverse momenta and $\vec{p}_T^{miss}$ to provide discrimination of signal from background. For a particle decaying to a visible and an invisible particle, the transverse mass (m_T) calculated from the $\vec{p}_T$ of the visible decay products should have a kinematic endpoint at the mass of the parent particle. Assuming that the p_T^{miss} corresponds to the p_T of the invisible particle, we calculate the m_T observable for the visible particle q and the invisible particle as follows:

$$m_T(q, \vec{p}_T^{miss}) \equiv \sqrt{2p_T^q p_T^{miss}[1 - \cos\Delta\phi(\vec{p}_T^q, \vec{p}_T^{miss})]}. \quad (1)$$

We use as a discriminant the sum of the transverse masses calculated for each τ_h with p_T^{miss}, Σm_T, given by

$$\Sigma m_T = m_T(\tau_h^{(1)}, \vec{p}_T^{miss}) + m_T(\tau_h^{(2)}, \vec{p}_T^{miss}). \quad (2)$$

Another variable found to be useful in the discrimination of signal from background is the "stransverse mass" m_{T2} [62–64]. This mass variable is a generalization of m_T in the case of multiple invisible particles. It serves as an estimator of the mass of pair-produced particles when both particles decay to a final state containing the same invisible particle. It is given by:

$$m_{T2} = \min_{\vec{p}_T^{X(1)} + \vec{p}_T^{X(2)} = \vec{p}_T^{miss}} \left[\max\left(m_T^{(1)}, m_T^{(2)}\right)\right], \quad (3)$$

where $\vec{p}_T^{X(i)}$ (with i=1, 2) are the unknown transverse momenta of the two undetected particles, X(1) and X(2), corresponding to the neutralinos in our signal models, and $m_T^{(i)}$ are the transverse masses obtained by pairing either of the two invisible particles with one of the two leptons. The minimization (min) is over the possible momenta of the invisible particles, taken to be massless, which are constrained to

Table 1 Ranges in m_{T2}, Σm_T, and N_j used to define the SRs used in the $\tau_h\tau_h$ analysis

m_{T2} [GeV]	25–50						>50					
Σm_T [GeV]	200–250		250–300		>300		200–250		250–300		>300	
N_j	0	≥1	0	≥1	0	≥1	0	≥1	0	≥1	0	≥1

add up to the $\vec{p}_T^{\,miss}$ in the event. For direct $\tilde{\tau}$ pair production, with each $\tilde{\tau}$ decaying to a τ lepton and a $\tilde{\chi}_1^0$, m_{T2} should be correlated with the mass difference between the $\tilde{\tau}$ and $\tilde{\chi}_1^0$. A large value of m_{T2} is thus common in signal events for models with larger $\tilde{\tau}$ masses and relatively rare in SM background events.

The SR definitions for the $\tau_h\tau_h$ analysis, shown in Table 1, are based on a cut-and-count analysis of the sample satisfying the baseline selections. The regions are defined through criteria imposed on m_{T2}, Σm_T, and the number of reconstructed jets in an event, N_j. The Σm_T and m_{T2} distributions of events in the $\tau_h\tau_h$ final state surviving the baseline selections are shown in Fig. 2. The distributions obtained for 2016 and 2017 data are combined. Separate sets of simulated events are used to model signal and background events in 2016 and 2017 data using the methods described in Sect. 3. In all distributions, the last bin includes overflow events. After applying a minimum requirement of $m_{T2} > 25$ GeV in all SRs, we subdivide events into low (25–50 GeV) and high (>50 GeV) m_{T2} regions, to improve the sensitivity to lower and higher $\tilde{\tau}$ mass signals, respectively. For each m_{T2} region, the Σm_T distribution is exploited to provide sensitivity for a large range of $\tilde{\tau}$ mass signals. We define three bins in Σm_T: 200–250, 250–300, and >300 GeV. Finally, we subdivide events in each m_{T2} and Σm_T region into the categories $N_j = 0$ and $N_j \geq 1$. This binning is beneficial as background events passing the SR kinematic selections are largely characterized by additional jet activity, while signal contains very few additional jets. The 0-jet category therefore provides nearly background-free SRs. However, we retain the SRs with $N_j \geq 1$ that are also expected to contain signal events with ISR or pileup jets.

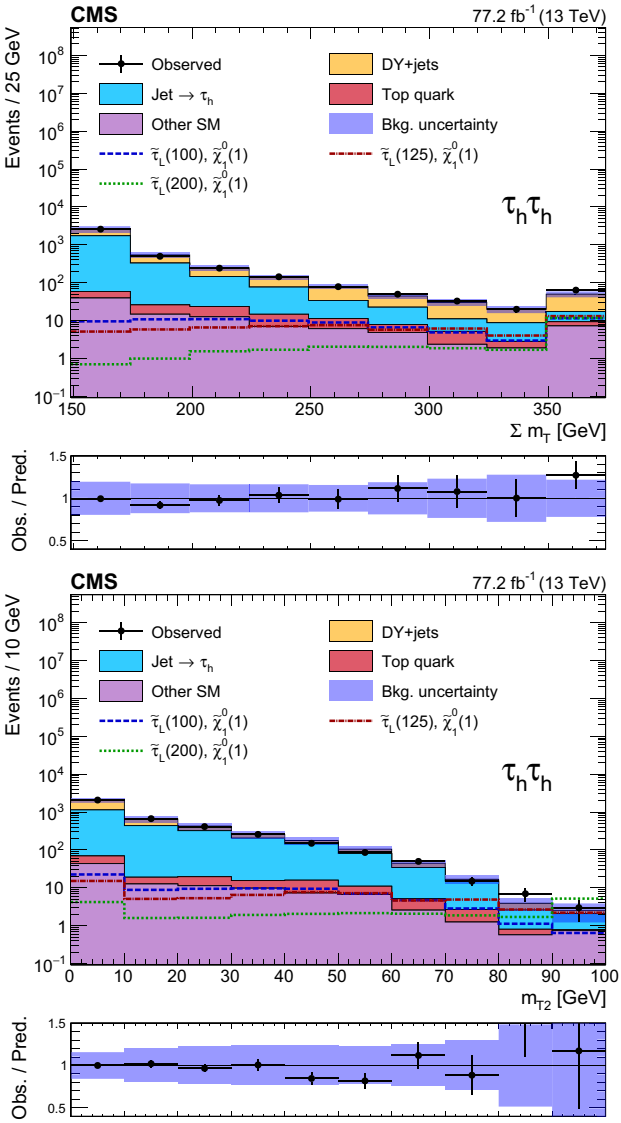

Fig. 2 Distributions in Σm_T (upper) and m_{T2} (lower) for events in the combined 2016 and 2017 data sets passing the baseline selection in the $\tau_h\tau_h$ final state, along with the corresponding prediction for the SM background and three benchmark models for $\tilde{\tau}_L$ pair production with $m(\tilde{\tau}_L) = 100$, 125, and 200 GeV, $m(\tilde{\chi}_1^0) = 1$ GeV. The numbers within parentheses in the legend correspond to the masses of the $\tilde{\tau}_L$ and $\tilde{\chi}_1^0$ in GeV. The last bin includes overflow events in each case. The shaded uncertainty bands represent the combined statistical and systematic uncertainties in the background

4.2 Event selection in the $\ell\tau_h$ final states

The baseline event selections for the $\ell\tau_h$ analyses require either an electron with $p_T > 26\,(35)$ GeV and $|\eta| < 2.1$ or a muon with $p_T > 25\,(28)$ GeV and $|\eta| < 2.4$ for the 2016 (2017) data, and a τ_h candidate with $p_T > 30$ GeV and $|\eta| < 2.3$. Electrons, muons, and τ_h candidates are required to have $|d_z| < 0.2$ cm, and electrons and muons are also required to have $|d_{xy}| < 0.045$ cm. Electrons and muons have to satisfy $I_{rel} < 0.15$ and <0.1, respectively. Backgrounds from $t\bar{t}$ and W+jets are greatly reduced by vetoing events that contain jets with $p_T > 20$ GeV. Events from the W+jets background are further reduced by requiring the transverse mass $m_T(\ell, \vec{p}_T^{\,miss})$, calculated using the electron or muon momentum vector and $\vec{p}_T^{\,miss}$, to be between 20 and 60 GeV or above 120 GeV. A significant background from DY+jets events is reduced by requiring the invariant mass of the electron or muon and the τ_h, $m_{\ell\tau_h}$ to be above 50 GeV.

To reduce background from QCD multijet events, we require $2.0 < \Delta R(\ell, \tau_h) < 3.5$.

With these preselection criteria in place, we train several BDTs corresponding to different signal hypotheses to classify signal and background events. The input variables are the p_T of the electron or muon, the p_T of the τ_h candidate, p_T^{miss}, $m_T(\ell, \vec{p}_T^{miss})$, $\Delta\eta(\ell, \tau_h)$, $\Delta\phi(\ell, \vec{p}_T^{miss})$, $\Delta\phi(\tau_h, \vec{p}_T^{miss})$, $\Delta R(\ell, \tau_h)$, $m(\ell\tau_h)$, and $m_T^{tot} \equiv \sqrt{m_T^2(\ell, \vec{p}_T^{miss}) + m_T^2(\tau_h, \vec{p}_T^{miss})}$. We also include m_{T2} and the contransverse mass (m_{CT}) [65,66], computed from the visible decay products and defined as

$$m_{CT} \equiv \sqrt{2 p_T^{\ell} p_T^{\tau_h} [1 + \cos \Delta\phi(\ell, \tau_h)]}. \quad (4)$$

For signal events, m_{CT} is expected to have an endpoint near $(m(\tilde{\tau})^2 - m(\tilde{\chi}_1^0)^2)/m(\tilde{\tau})$. Finally, we include the variable $D_\zeta = \vec{p}_T^{miss} \cdot \vec{\zeta} - 0.85(\vec{p}_T^{\ell} + \vec{p}_T^{\tau_h}) \cdot \vec{\zeta}$, with $\vec{\zeta}$ being the bisector of the directions of the transverse momenta of the electron or muon and the τ_h candidate [67,68]. The value of 0.85 reflects an optimization to efficiently distinguish DY+jets events from other backgrounds and the signal. Figure 3 shows the distributions of events passing the baseline selections in the $\mu\tau_h$ final state in two of the BDT input variables that provide the highest discriminating power, p_T^{miss} and m_T^{tot}. The distributions observed in the $e\tau_h$ final state are similar.

Since the signal kinematics depend on mass, we train BDTs for signals with $\tilde{\tau}$ masses of 100, 150, and 200 GeV. In all cases we use a $\tilde{\chi}_1^0$ mass of 1 GeV. As the results of the training depend critically on the number of input events, we relax the τ_h MVA-based isolation criteria and reduce the p_T threshold for the τ_h to 20 GeV for the training sample in order to increase the number of training and test events. The "very tight" isolation and a p_T threshold of 30 GeV for the τ_h are applied in the final analysis. For a given signal hypothesis, we choose the BDT trained with the same $\tilde{\tau}$ mass for models with $\tilde{\tau}$ masses of 100, 150, and 200 GeV, or the one that provides optimal sensitivity for models with other $\tilde{\tau}$ mass values. For signal models with $\tilde{\tau}$ masses of 90 and 125 GeV, we use the BDT trained for $m(\tilde{\tau}) = 100$ GeV, while for those with a $\tilde{\tau}$ mass of 175 GeV, we use the BDT trained for $m(\tilde{\tau}) = 200$ GeV. While signal events are largely expected to have high BDT output values, we include the full BDT distribution in a binned fit for the statistical interpretation of the analysis as described in Sect. 7. The binning is chosen to optimize signal significance.

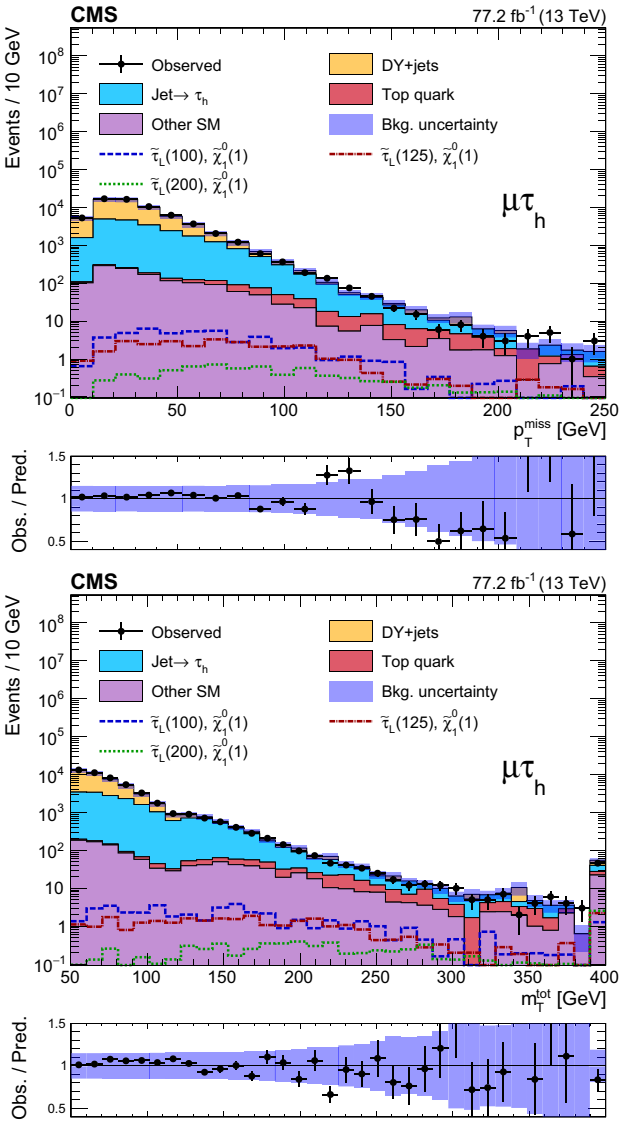

Fig. 3 Distributions in p_T^{miss} (upper) and m_T^{tot} (lower) for events in the combined 2016 and 2017 data passing the baseline selections in the $\mu\tau_h$ final state, along with the corresponding prediction for SM background and three benchmark models of $\tilde{\tau}_L$ pair production with $m(\tilde{\tau}_L) = 100$, 125, and 200 GeV and $m(\tilde{\chi}_1^0) = 1$ GeV. The numbers within parentheses in the legend correspond to the masses of the $\tilde{\tau}_L$ and $\tilde{\chi}_1^0$ in GeV. The last bin includes overflow events in each case. The shaded uncertainty bands represent the combined statistical and average systematic uncertainties in the background

5 Background estimation

Our most significant backgrounds are from DY+jets, W+jets, QCD multijet, $t\bar{t}$, and diboson processes. They have relative contributions that vary with final state. For the $\tau_h\tau_h$ final state, the dominant background arises from the misidentification of jets as τ_h candidates in QCD multijet and W+jets events, constituting ≈65% of background after the baseline selection. For the $\ell\tau_h$ final states after the baseline selection, the main backgrounds are from DY+jets (≈50%), W+jets (≈30%), and QCD multijet (≈10%) events. The DY+jets contribution, which is also a major background in the $\tau_h\tau_h$ final state (≈20%), usually consists of events with two prompt τ leptons. This background is determined with

simulation samples after applying corrections to match the normalization and to be consistent with variable distributions in collider data. The W+jets and QCD multijet backgrounds usually contain one or more jets misidentified as τ_h and their contributions are determined via methods that rely on data. Finally, we have smaller contributions from other SM processes such as the production of Higgs bosons, dibosons, and top quark pairs with or without vector bosons. These are estimated via MC simulation with appropriate correction factors applied as described in Sect. 3. For the $\ell\tau_h$ analyses, dedicated CRs that are each enriched in one of the major background processes are used to validate the modeling of the BDT distribution and to extract uncertainties that are used to account for any potential mismodeling of the distributions in simulation. These CRs are described in the following subsections below.

5.1 Estimation of background from misidentified jets

5.1.1 Misidentified jets in the $\tau_h\tau_h$ final state

After requiring two τ_h candidates with high p_T, events with misidentified τ_h candidates are the dominant background in the $\tau_h\tau_h$ final state. This background, which originates predominantly from QCD multijet and W+jets production, is predicted by extrapolating the event count in a data sample selected with a relaxed isolation requirement into the SR. The fraction of non-prompt or misidentified τ_h candidates selected with the very loose MVA-based isolation working point that also pass the tight DeepPF isolation requirement is measured in a QCD multijet-enriched sample of same-charge $\tau_h\tau_h$ events. The same-charge $\tau_h\tau_h$ events are collected with the same $\tau_h\tau_h$ trigger as opposite-charge $\tau_h\tau_h$ events to avoid additional trigger-related biases. We also require m_{T2} to be low (<40 GeV) to reduce potential contributions from signal events. We find that roughly 20% of the same-charge events with misidentified τ_h candidates selected with very loose isolation also pass the tight isolation requirement. However, the rate depends on the p_T and decay mode (one- or three-prongs) of the τ_h candidate, as well as the jet flavor, i.e., whether the misidentified jet originates from the hadronization of light-flavor quarks, heavy-flavor quarks, or gluons. The τ_h misidentification rate is therefore measured in bins of p_T and decay mode to mitigate the dependence on these factors. The measurement is also binned in the number of primary vertices (N_{PV}) to capture the effects of pileup. From studies performed with MC simulation samples, a systematic uncertainty of ≈30% is assigned to account for the dependence of the misidentification rate on jet flavor.

Since the isolation efficiency for prompt τ_h candidates is only around 70–80%, processes containing genuine τ_h candidates can enter the sideband regions in events that are selected with the relaxed isolation requirement. To take this into account when calculating the final background estimate, we define three categories of events with at least two loosely isolated τ_h candidates: (1) events in which both τ_h candidates pass the tight DeepPF isolation requirement, (2) events in which one passes and one fails the tight isolation requirement, and (3) events in which both τ_h candidates fail the tight isolation requirement. We then equate the count of events in each of these three event categories to the sum of expected counts for the events with two prompt τ_h candidates, two jets misidentified as τ_h candidates, or one prompt τ_h candidate

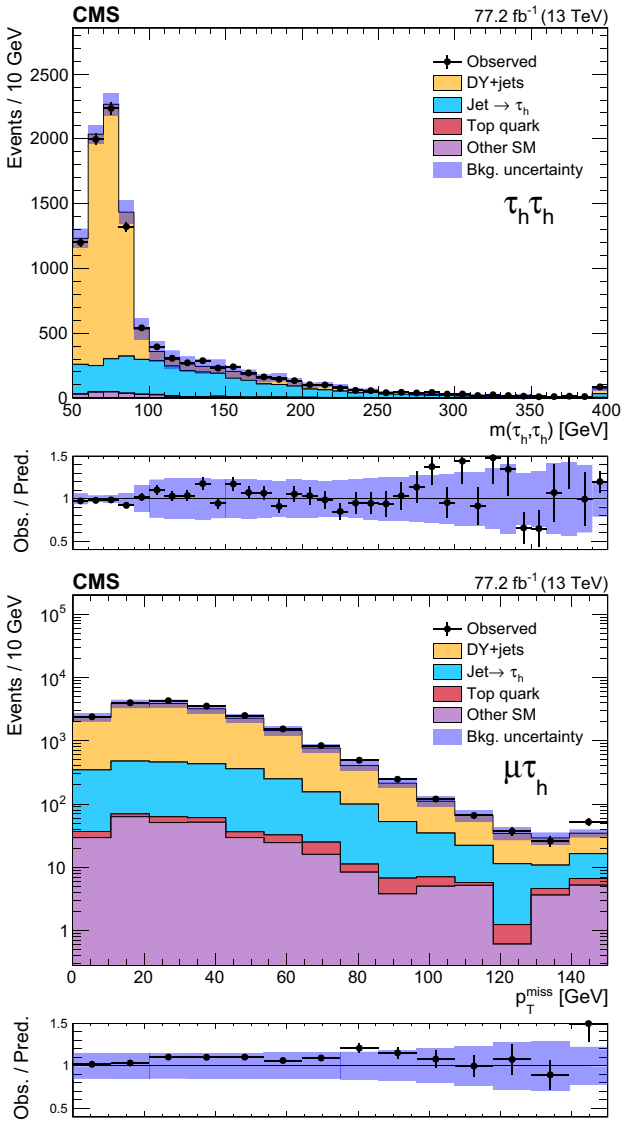

Fig. 4 Visible-mass spectra of τ lepton pairs in $\tau_h\tau_h$ events (upper) and p_T^{miss} distribution in $\mu\tau_h$ events (lower) in data and the corresponding prediction for SM background in the combined 2016 and 2017 DY+jets validation regions. The last bin includes overflow events in each case. The shaded uncertainty band represents the statistical and systematic uncertainties in the background prediction. For the $\mu\tau_h$ distribution, the systematic uncertainty included in each bin corresponds to a single common average value

Table 2 Systematic uncertainties of SM background predictions and a representative signal model, corresponding to a left-handed $\tilde{\tau}$, with $m(\tilde{\tau}) = 100\,\text{GeV}$ and $m(\tilde{\chi}_1^0) = 1\,\text{GeV}$. The uncertainty ranges are given in percent. The spread of values reflects uncertainties in different SRs

Uncertainty (%)	Signal	Misidentified τ_h	DY+jets	Top quark	Other SM
τ_h efficiency	5–13	–	5–15	1–14	10–51
e/μ efficiency ($\ell\tau_h$)	2–3	–	2–3	2–3	2–3
τ_h energy scale	0.5–12	–	2.6–27	1.2–11	4.1–13
e/μ energy scale ($\ell\tau_h$)	0.1–25	0.1–5	0.1–30	0.1–20	0.1–10
Jet energy scale	0.5–38	–	1.1–19	0.6–13	2.4–14
Jet energy resolution	0.3–22	–	1.9–10	0.7–22	0.2–11
Unclustered energy	0.3–21	–	2.6–30	0.2–6.4	1.7–14
b tagging	0.2–0.9	–	0.2–23	1.7–25	0.2–1.2
Pileup	0.9–9.1	–	2–22	0.1–24	0.3–25
BDT distribution ($\ell\tau_h$)	9	–	9	9	9
$\ell \to \tau_h$ misidentification rate ($\ell\tau_h$)	–	–	–	1	1
Integrated luminosity	2.3–2.5	–	2.3–2.5	2.3–2.5	2.3–2.5
Background normalization	–	10	5–15	2.5–15	15–25
DY+jets mass and p_T	–	–	0.2–11	–	–
τ_h misidentification rate	–	4.6–51	–	–	–
Signal ISR	0.2–8.2	–	–	–	–
Renormalization and factorization scales	1.6–7	–	0.7–14	0.7–30	6.7–16
PDFs	–	–	0.1–1.2	0.1–0.4	0.1–0.6

and one jet misidentified as a τ_h candidate, that contribute to each category. The contributions from backgrounds with one or two jets misidentified as τ_h candidates in the SRs are then determined analytically by solving a set of linear equations.

5.1.2 *Misidentified jets in the $e\tau_h$ and $\mu\tau_h$ final states*

The misidentification of jets as τ_h candidates also gives rise to a major source of background in the $e\tau_h$ and $\mu\tau_h$ final states that arises mainly from W+jets events with leptonic W boson decays. We estimate this background from a sideband region in data selected using the SR selection criteria, with the exception that the τ_h candidates are required to satisfy the loose isolation working point and not the very tight working point. A transfer factor for the extrapolation of event counts from this τ_h-isolation range into the tight isolation range of the SR is determined with a W+jets CR selected from events with one muon and at least one τ_h candidate that passes the loose isolation requirement. In events with more than one τ_h candidate, the candidate with the highest value of the MVA-based isolation discriminant is used. To increase the purity of W+jets events in this region, we reduce the contribution from $\mathrm{t\bar{t}}$ and QCD multijet events by requiring $60 < m_T(\ell, \vec{p}_T^{\,\text{miss}}) < 120\,\text{GeV}$, $p_T^{\text{miss}} > 40\,\text{GeV}$, no more than two jets, and an azimuthal separation of at least 2.5 radians between any jet and the W boson reconstructed from the muon and $\vec{p}_T^{\,\text{miss}}$ ($\Delta\phi(\text{W, jet}) > 2.5$). We also reject events with additional electrons or muons satisfying looser identification criteria. The remaining sample has an expected purity of $\approx 85\%$ for W+jets events. The transfer factor, R, is then determined from this control sample after subtracting the remaining non-W+jets background contributions estimated from simulation, as follows:

$$R = \frac{N_{\text{data}}^{\text{CR}}(\text{VT}) - N_{\text{MC no W}}^{\text{CR}}(\text{VT})}{N_{\text{data}}^{\text{CR}}(\text{L}\overline{\text{VT}}) - N_{\text{MC no W}}^{\text{CR}}(\text{L}\overline{\text{VT}})}, \tag{5}$$

where $N_{\text{data}}^{\text{CR}}$ corresponds to the number of events in the CR in data. The parenthetical argument VT denotes events in which the τ_h candidate satisfies the very tight isolation working point, while $\text{L}\overline{\text{VT}}$ denotes those that satisfy the loose, but not the very tight requirement. Transfer factors are determined separately in bins of p_T and η of τ_h candidates in order to achieve an accurate description of the background.

The contribution of the background originating from a jet misidentified as a τ_h candidate in the SR is then determined from the corresponding sideband in data:

$$N(\text{jet} \to \tau_h) = R\,(N_{\text{data}}^{\text{sideband}} - N_{\text{MC},\tau}^{\text{sideband}}), \tag{6}$$

where $N_{\text{data}}^{\text{sideband}}$ is the number of events in the sideband in data, from which $N_{\text{MC},\tau}^{\text{sideband}}$, the number with genuine τ leptons as estimated with MC simulation by generator-level matching, is subtracted. We validate the estimation of jets misidentified as τ_h in a CR requiring $60 < m_T(\ell, \vec{p}_T^{\,\text{miss}}) < 120\,\text{GeV}$ and $\Delta\phi(\text{W, jet}) < 2.5$ to ensure that the region

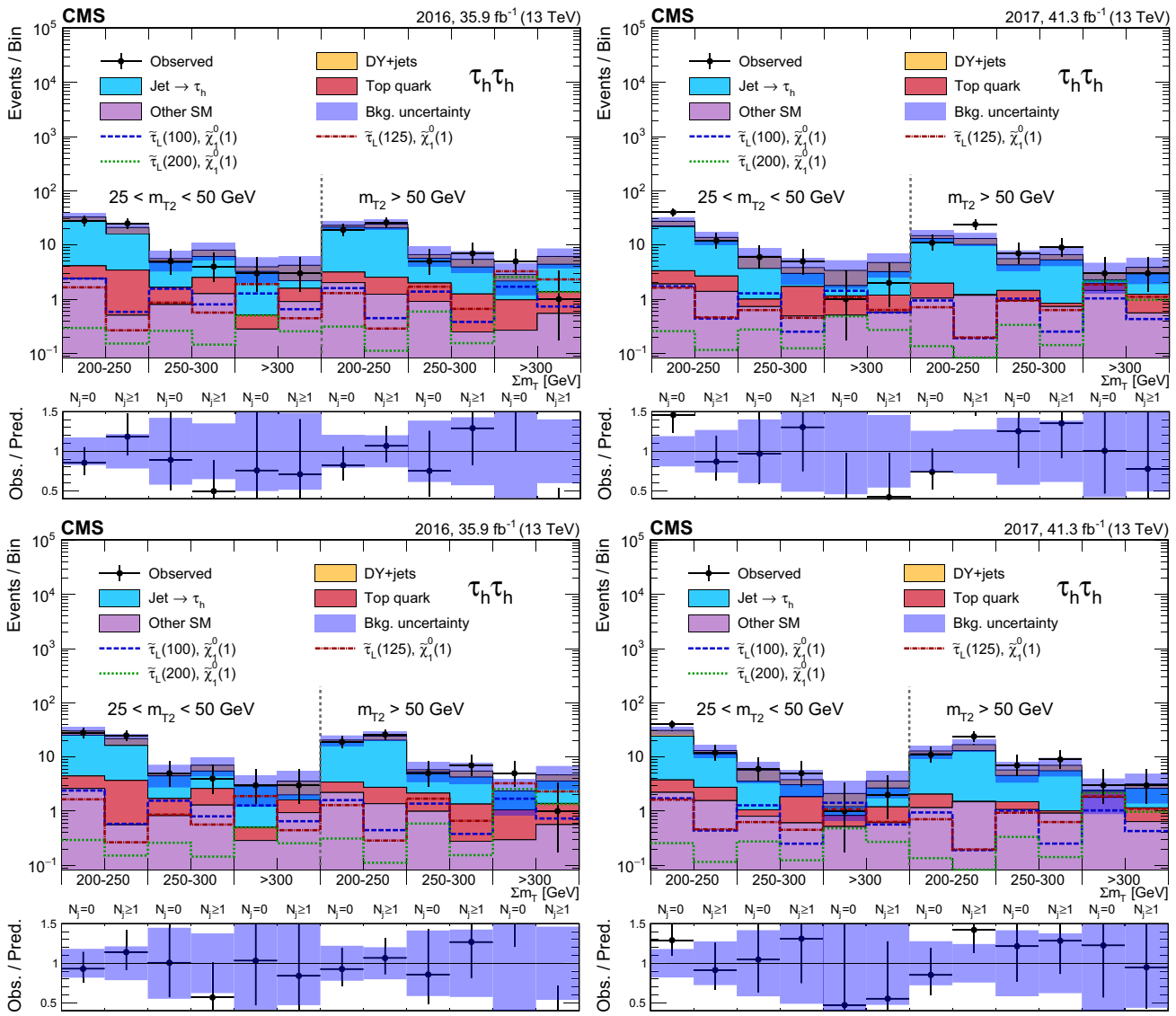

Fig. 5 Event counts and predicted yields for the SM background in the $\tau_h\tau_h$ analysis for the 2016 (left) and 2017 (right) data, before (upper) and after (lower) a maximum-likelihood fit to the data. Predicted signal yields are also shown for benchmark signal models of $\tilde{\tau}_L$ pair production with $m(\tilde{\tau}_L) = 100$, 125, and 200 GeV and $m(\tilde{\chi}_1^0) = 1$ GeV

is independent of the region described above that is used to estimate the background.

5.2 Estimation of background from Drell–Yan+jets

The DY+jets background comes primarily from $Z \to \tau^+\tau^-$ decays. We estimate this contribution via simulation, after applying corrections based on CRs in data. Mismodeling of the Z boson mass or p_T distribution in simulation can lead to significant differences between data and simulation in kinematic discriminant distributions, especially when considering the large values of these variables that are relevant for the $\tau_h\tau_h$ SRs. We therefore use a high-purity $Z \to \mu^+\mu^-$ CR to compare the dimuon mass and p_T spectra between data and simulation and use the observed differences to correct the simulation in the SRs with weights parameterized by generator-level Z boson mass and p_T. The correction factors range up to 30% for high-mass and high-p_T values. Because these factors are intended to compensate for missing higher-order effects in the simulation, we assign the differences between the generator-level Z boson mass and p_T distributions in LO and NLO simulated events as systematic uncertainties. The differences between data and simulation are taken into account through the use of scale factors, as described in Sect. 3. The uncertainties in these corrections are propagated to the final background estimate. The cor-

Table 3 Predicted background yields and observed event counts in $\tau_h\tau_h$ SRs in 2016 data. For the background estimates with no events in the sideband or in the simulated sample, we calculate the 68% CL upper limit on the yield. The first and second uncertainties given are statistical and systematic, respectively. We also list the predicted signal yields corresponding to the purely left-handed model for a $\tilde{\tau}$ mass of 100 GeV and a $\tilde{\chi}_1^0$ mass of 1 GeV

m_{T2} [GeV]	25–50					
Σm_T [GeV]	200–250		250–300		>300	
N_j	0	≥1	0	≥1	0	≥1
Misidentified τ_h	$23.5 \pm 2.9 \pm 9.8$	$12.7 \pm 2.4 \pm 4.2$	$3.1 \pm 1.0 \pm 1.7$	$3.6 \pm 1.1 \pm 2.0$	$2.8 \pm 0.8 \pm 1.8$	$0.5 \pm 0.5 \pm 0.2$
DY+jets	$4.3 \pm 2.1 \pm 0.7$	$4.5 \pm 1.5 \pm 0.9$	$0.4 \pm 0.4 \pm 0.1$	$1.6 \pm 0.9 \pm 0.3$	< 0.7	$1.5 \pm 0.9 \pm 0.5$
Top quark	$1.7 \pm 0.3 \pm 0.3$	$2.9 \pm 0.4 \pm 0.3$	$0.8 \pm 0.2 \pm 0.1$	$1.3 \pm 0.2 \pm 0.2$	$0.2 \pm 0.1 \pm 0.1$	$0.6 \pm 0.2 \pm 0.2$
Other SM	$2.4 \pm 0.7 \pm 0.4$	$0.5 \pm 0.2 \pm 0.1$	$0.7 \pm 0.4 \pm 0.1$	$1.2 \pm 0.5 \pm 0.3$	$0.3 \pm 0.2 \pm 0.1$	$0.9 \pm 0.4 \pm 0.2$
Total prediction	$31.9 \pm 3.7 \pm 9.8$	$20.6 \pm 2.9 \pm 4.3$	$5.1 \pm 1.2 \pm 1.7$	$7.7 \pm 1.5 \pm 2.1$	$3.2 \pm 0.9 \pm 1.8$	$3.5 \pm 1.1 \pm 0.6$
Observed	28	25	5	4	3	3
$m(\tilde{\tau}_L) = 100$ GeV	$2.4 \pm 0.3 \pm 0.4$	$0.6 \pm 0.2 \pm 0.1$	$1.6 \pm 0.2 \pm 0.2$	$0.8 \pm 0.2 \pm 0.1$	$1.3 \pm 0.2 \pm 0.4$	$0.7 \pm 0.2 \pm 0.2$
m_{T2} [GeV]	>50					
Σm_T [GeV]	200–250		250–300		>300	
N_j	0	≥1	0	≥1	0	≥1
Misidentified τ_h	$18.2 \pm 2.8 \pm 9.5$	$18.1 \pm 2.9 \pm 6.0$	$3.7 \pm 1.0 \pm 2.2$	$2.7 \pm 1.1 \pm 0.5$	$1.1 \pm 0.6 \pm 0.6$	$2.9 \pm 0.8 \pm 1.6$
DY+jets	$1.1 \pm 0.8 \pm 0.2$	$3.3 \pm 1.3 \pm 0.7$	$0.5 \pm 0.5 \pm 0.1$	$1.0 \pm 0.7 \pm 0.1$	< 0.7	$1.3 \pm 0.8 \pm 0.5$
Top quark	$1.1 \pm 0.3 \pm 0.1$	$1.3 \pm 0.2 \pm 0.3$	$1.1 \pm 0.2 \pm 0.2$	$1.0 \pm 0.2 \pm 0.1$	$0.7 \pm 0.2 \pm 0.1$	$0.8 \pm 0.2 \pm 0.1$
Other SM	$2.0 \pm 0.6 \pm 0.3$	$1.2 \pm 0.4 \pm 0.2$	$0.9 \pm 0.4 \pm 0.1$	$0.2 \pm 0.1 \pm 0.1$	$0.3 \pm 0.1 \pm 0.1$	$0.5 \pm 0.2 \pm 0.2$
Total prediction	$22.5 \pm 3.0 \pm 9.5$	$23.9 \pm 3.3 \pm 6.0$	$6.2 \pm 1.2 \pm 2.2$	$4.9 \pm 1.3 \pm 0.5$	$2.1 \pm 0.6 \pm 0.6$	$5.5 \pm 1.2 \pm 1.7$
Observed	19	26	5	7	5	1
$m(\tilde{\tau}_L) = 100$ GeV	$1.6 \pm 0.2 \pm 0.3$	$0.4 \pm 0.1 \pm 0.1$	$1.4 \pm 0.2 \pm 0.2$	$0.4 \pm 0.1 \pm 0.1$	$1.7 \pm 0.2 \pm 0.4$	$0.7 \pm 0.2 \pm 0.2$

rected simulation is validated in the $\tau_h\tau_h$ final state using a $Z \to \tau^+\tau^-$ CR selected by inverting the m_{T2} and Σm_T requirements used to define the SRs. In addition, requiring a p_T of at least 50 GeV for the $\tau_h\tau_h$ system reduces the QCD multijet background and improves the purity of this CR. This choice makes it possible to increase the statistical power of this region by removing the $p_T^{miss} > 50$ GeV requirement. The visible mass distribution of the $\tau_h\tau_h$ system shown in Fig. 4 (upper) demonstrates that the corrected simulation agrees with the data within experimental uncertainties.

For the analysis in the $\ell\tau_h$ final states, a normalization scale factor, as well as corrections to the p_T distribution of the Z boson in simulation are obtained from a very pure $Z \to \mu^+\mu^-$ CR in data. These events are selected by requiring two isolated muons and no additional leptons, at most one jet, no b-tagged jets, and a dimuon mass in a window of 75–105 GeV, to increase the probability to >99% that they originate from $Z \to \mu^+\mu^-$ decays. After subtracting all other contributions estimated from simulation, a normalization scale factor of 0.96 ± 0.05, which is compatible with unity, is extracted from the ratio of data to simulated events. The uncertainty in the scale factor is determined by varying systematic uncertainties associated with objects such as the muon efficiency and jet energy uncertainties.

To validate the DY+jets background prediction in the $\ell\tau_h$ analyses, we construct a CR in $\mu\tau_h$ events with $m_T(\mu, \vec{p}_T^{miss}) < 20$ GeV, $50 < m(\mu\tau_h) < 80$ GeV, and $N_j = 0$. These requirements are chosen to obtain a $Z \to \tau^+\tau^-$ sample with good purity. The $m(\mu\tau_h)$ range is chosen to select the Z boson peak, low $m_T(\mu, \vec{p}_T^{miss})$ helps to remove W+jets and potential signal contamination while the 0-jet requirement helps remove other backgrounds. The p_T^{miss} distribution of these events is shown in Fig. 4 (lower). We observe good agreement between data and the predicted background.

5.3 Estimation of other backgrounds

Smaller contributions are expected from other SM backgrounds, including diboson, triboson, and Higgs boson production. There are also contributions from $t\bar{t}$ and single top quark production, or top quark pair production in association with a vector boson. These are estimated via MC simulation after application of efficiency and energy-scale corrections. Experimental and theoretical uncertainties are evaluated as described below in Sect. 6.

For the $\ell\tau_h$ analyses, we check the BDT distribution in a $t\bar{t}$-enriched CR that is defined by requiring the event selection

Table 4 Predicted background yields and observed event counts in $\tau_h\tau_h$ SRs in 2017 data. For the background estimates with no events in the sideband or in the simulated sample, we calculate the 68% CL upper limit on the yield. The first and second uncertainties given are statistical and systematic, respectively. We also list the predicted signal yields corresponding to the purely left-handed model for a $\widetilde{\tau}$ mass of 100 GeV and a $\widetilde{\chi}_1^0$ mass of 1 GeV

m_{T2} [GeV]	25–50					
Σm_T [GeV]	200–250		250–300		>300	
N_j	0	≥1	0	≥1	0	≥1
Misidentified τ_h	$18.6 \pm 3.1 \pm 3.6$	$9.4 \pm 2.1 \pm 1.7$	$2.7 \pm 0.9 \pm 1.0$	$1.1 \pm 0.8 \pm 0.3$	$0.5 \pm 0.5 \pm 0.1$	$1.9 \pm 0.8 \pm 1.3$
DY+jets	$5.0 \pm 2.0 \pm 0.7$	$1.5 \pm 0.7 \pm 0.2$	$1.9 \pm 1.4 \pm 0.5$	$0.6 \pm 0.4 \pm 0.2$	$1.1 \pm 0.8 \pm 0.3$	$1.0 \pm 0.8 \pm 0.1$
Top quark	$1.2 \pm 0.6 \pm 0.2$	$1.1 \pm 0.5 \pm 0.2$	$0.2 \pm 0.1 \pm 0.1$	$1.0 \pm 0.6 \pm 0.1$	$0.3 \pm 0.3 \pm 0.1$	$0.5 \pm 0.2 \pm 0.1$
Other SM	$1.9 \pm 0.7 \pm 0.4$	$1.4 \pm 0.6 \pm 0.4$	$0.7 \pm 0.5 \pm 0.1$	$0.5 \pm 0.5 \pm 0.1$	$0.5 \pm 0.3 \pm 0.1$	$0.6 \pm 0.4 \pm 0.3$
Total prediction	$26.7 \pm 3.8 \pm 3.7$	$13.3 \pm 2.3 \pm 1.8$	$5.5 \pm 1.8 \pm 1.1$	$3.2 \pm 1.2 \pm 0.4$	$2.4 \pm 1.0 \pm 0.4$	$4.0 \pm 1.2 \pm 1.4$
Observed	40	12	6	5	1	2
$m(\widetilde{\tau}_L) = 100\,\text{GeV}$	$1.7 \pm 0.2 \pm 0.2$	$0.4 \pm 0.1 \pm 0.1$	$1.3 \pm 0.2 \pm 0.2$	$0.3 \pm 0.1 \pm 0.1$	$1.4 \pm 0.2 \pm 0.4$	$0.6 \pm 0.1 \pm 0.2$
m_{T2} [GeV]	>50					
Σm_T [GeV]	200–250		250–300		>300	
N_j	0	≥1	0	≥1	0	≥1
Misidentified τ_h	$11.2 \pm 2.3 \pm 4.7$	$9.0 \pm 2.6 \pm 1.1$	$2.8 \pm 1.3 \pm 0.3$	$4.5 \pm 1.4 \pm 1.8$	$0.2 \pm 0.7 \pm 0.5$	$1.6 \pm 0.8 \pm 0.2$
DY+jets	$1.3 \pm 0.8 \pm 0.2$	$2.6 \pm 1.0 \pm 0.4$	$1.0 \pm 0.6 \pm 0.1$	$1.0 \pm 0.6 \pm 0.1$	< 0.7	$0.5 \pm 0.5 \pm 0.1$
Top quark	$0.8 \pm 0.4 \pm 0.1$	< 0.2	$0.3 \pm 0.3 \pm 0.1$	$0.1 \pm 0.1 \pm 0.1$	$0.4 \pm 0.3 \pm 0.1$	$0.6 \pm 0.5 \pm 0.2$
Other SM	$1.0 \pm 0.4 \pm 0.2$	$1.2 \pm 0.6 \pm 0.2$	$0.9 \pm 0.5 \pm 0.1$	$0.7 \pm 0.5 \pm 0.1$	$1.4 \pm 0.7 \pm 0.3$	$0.6 \pm 0.4 \pm 0.2$
Total prediction	$14.3 \pm 2.5 \pm 4.7$	$12.8 \pm 2.8 \pm 1.2$	$5.1 \pm 1.5 \pm 0.3$	$6.3 \pm 1.6 \pm 1.8$	$2.0 \pm 1.0 \pm 0.6$	$3.2 \pm 1.1 \pm 0.4$
Observed	11	24	7	9	3	3
$m(\widetilde{\tau}_L) = 100\,\text{GeV}$	$0.9 \pm 0.2 \pm 0.1$	$0.2 \pm 0.1 \pm 0.1$	$1.0 \pm 0.2 \pm 0.2$	$0.3 \pm 0.1 \pm 0.1$	$1.0 \pm 0.2 \pm 0.2$	$0.4 \pm 0.1 \pm 0.1$

to be the same as in the SR, except for a requirement of one or two b-tagged jets. To validate the WW background prediction, we construct a CR of events with oppositely charged muon-electron pairs that have $m_{\mu e} > 90\,\text{GeV}$ and $N_j = 0$. We obtain systematic uncertainties for the normalization of the corresponding backgrounds and any potential mismodeling of the BDT distribution in these CRs. The latter is done by constructing a χ^2 test for all CRs with the BDT modeling taken into account by including an additional floating uncertainty that is determined by requiring a p value [69] of at least 68% in all CRs. In this way, the BDT shape uncertainty is estimated to be 9%.

6 Systematic uncertainties

The dominant uncertainties in this analysis are the statistical uncertainties resulting from limited event counts in data sidebands or in simulated event samples used to obtain background estimates and the systematic uncertainties in the estimated rates for jets to be misidentified as τ_h candidates. We rely on an extrapolation in τ_h isolation to obtain an estimate of the background originating from jets misidentified as τ_h candidates. In the $\tau_h\tau_h$ analysis, the uncertainty in this extrapolation is dominated by the dependence of isolation on jet flavor. It also includes the statistical uncertainty associated with the CR samples from which the extrapolation factors are obtained, which can be significant in the case of search regions with limited event counts that are defined with stringent kinematic requirements. The uncertainty in the combined identification and isolation efficiency for prompt τ_h candidates is also propagated to the final estimated uncertainty. In the $\ell\tau_h$ analyses, we estimate a transfer factor for the extrapolation in τ_h isolation from a W+jets-enriched CR. The purity of W+jets events this region is ≈85% as determined from simulation. We therefore propagate a relative uncertainty of 15% to account for contamination from other sources.

We use simulation to obtain estimates of the yields from other background contributions and to estimate the potential signal contributions. We propagate uncertainties related to the b tagging, trigger, and selection efficiencies, the renormalization and factorization scales, PDFs, jet energy scale and resolution, unclustered energy contributing to p_T^{miss}, and the energy scales of electrons, muons, and τ_h candidates. The correction factors and the corresponding uncertainties for the τ_h energy scale in simulation are derived from $Z \to \tau^+\tau^-$ events in the $\ell\tau_h$ final states by fits

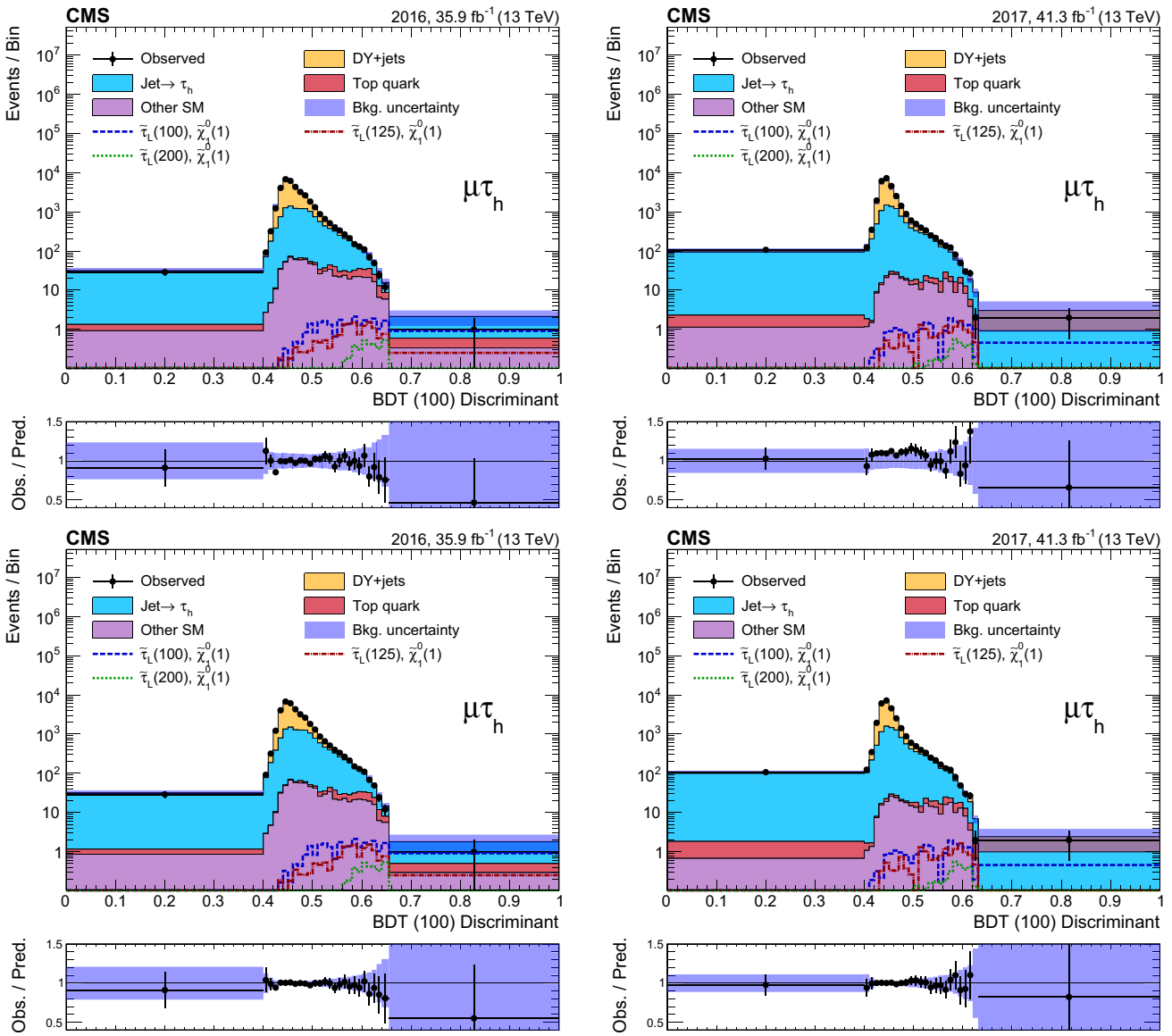

Fig. 6 Discriminant distributions for the BDT trained for a $\tilde{\tau}$ mass of 100 GeV and a $\tilde{\chi}_1^0$ mass of 1 GeV (BDT (100)) in the $\mu\,\tau_h$ final state for the 2016 (left) and 2017 (right) data, before (upper) and after (lower) a maximum-likelihood fit to the data. Predicted signal yields are also shown for benchmark models of $\tilde{\tau}_L$ pair production with $m(\tilde{\tau}_L) = 100$, 125, and 200 GeV and $m(\tilde{\chi}_1^0) = 1$ GeV

to distributions of the reconstructed τ_h mass and the visible mass of the $\ell\tau_h$ system [48]. The systematic uncertainties corresponding to energy scale variations can be significant in the $\tau_h\tau_h$ search regions defined with stringent kinematic requirements, which are affected by large statistical uncertainties, because of potentially large event migrations. For the DY+jets background, we have an additional uncertainty associated with the corrections applied to the mass and p_T distributions. We assign a 15% normalization uncertainty in the $\tau_h\tau_h$ final state for the cross sections of processes estimated from simulation, namely DY+jets, $t\bar{t}$, diboson, and rare SM processes, based on the results of CMS differential cross section measurements [70,71]. For the $\ell\tau_h$ analyses, we extract normalization uncertainties of 5, 5, and 20% for the DY+jets, $t\bar{t}$, and WW backgrounds, respectively, based on the estimated impurity of the corresponding process-enriched CRs. An additional uncertainty of 9% is assigned to cover potential mismodeling of the BDT distribution in simulation that is based on studies in CRs.

The categorization of events in the $\tau_h\tau_h$ final state by the number of reconstructed jets induces sensitivity to the modeling of ISR in the signal simulation. The p_T^{ISR} distribution of simulated signal events is reweighted to improve the ISR

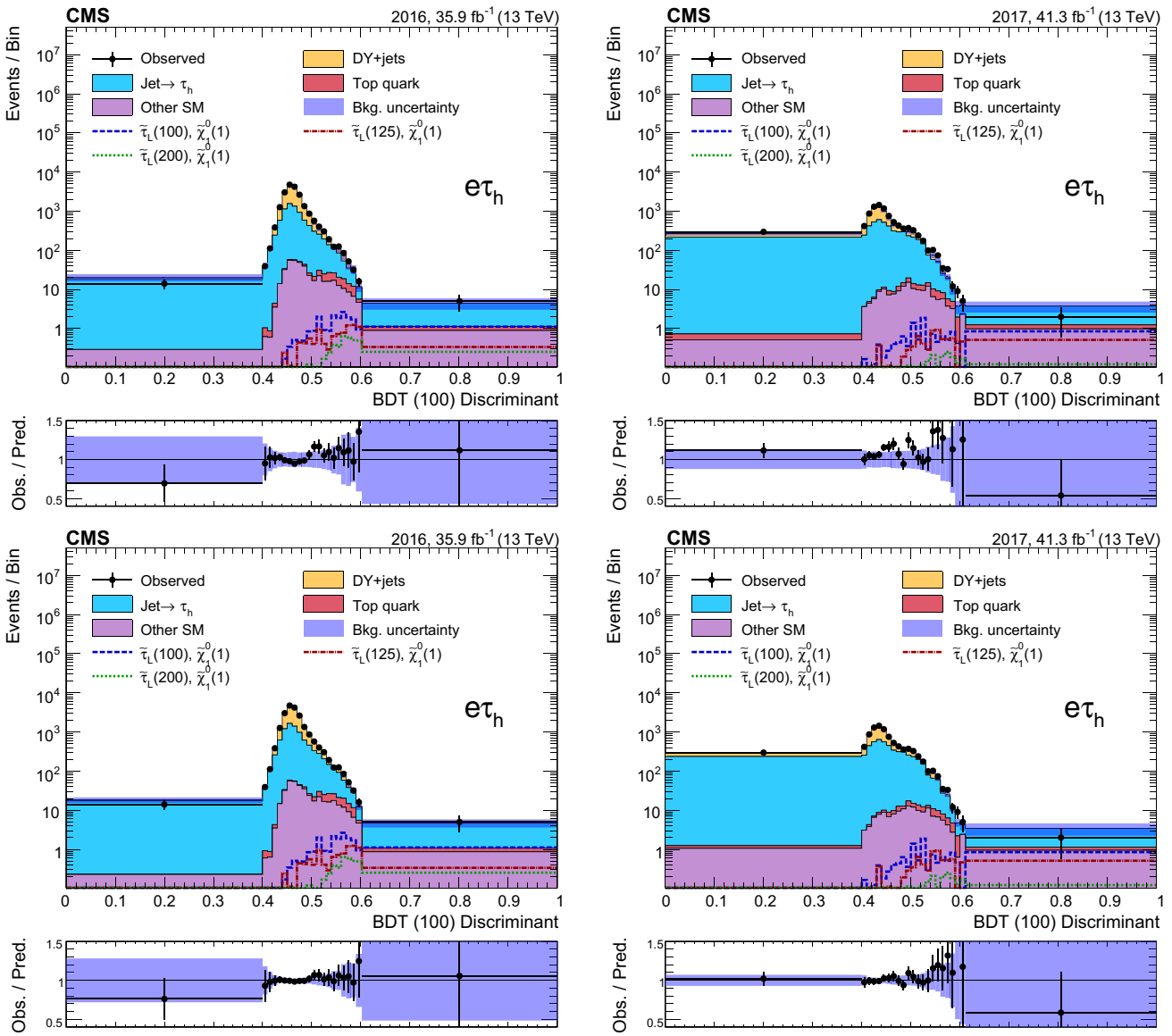

Fig. 7 Discriminant distributions for the BDT trained for a $\tilde{\tau}$ mass of 100 GeV and a $\tilde{\chi}_1^0$ mass of 1 GeV (BDT (100)) in the $e\tau_h$ final state for the 2016 (left) and 2017 (right) data, before (upper) and after (lower) a maximum-likelihood fit to the data. Predicted signal yields are also shown for benchmark models of $\tilde{\tau}_L$ pair production with $m(\tilde{\tau}_L) = 100$, 125, and 200 GeV and $m(\tilde{\chi}_1^0) = 1$ GeV

Table 5 Predicted background yields and observed event counts in the most sensitive last bins of the BDT distributions in the $e\tau_h$ and $\mu\tau_h$ final states, in data collected in 2016. The numbers in parentheses in the first row are the $\tilde{\tau}$ and $\tilde{\chi}_1^0$ masses corresponding to the signal model for left-handed $\tilde{\tau}$ pair production that is used to train the BDT. In the bottom row, we list the corresponding predicted signal yields in the last bin of the BDT distribution. The first and second uncertainties given are statistical and systematic, respectively

BDT training	BDT($\mu\tau_h$,100,1)	BDT($\mu\tau_h$,150,1)	BDT($\mu\tau_h$,200,1)	BDT($e\tau_h$,100,1)	BDT($e\tau_h$,150,1)	BDT($e\tau_h$,200,1)
Misidentified τ_h	$1.6 \pm 0.8 \pm 0.3$	$2.3 \pm 1.0 \pm 0.4$	$1.5 \pm 0.8 \pm 0.3$	$3.3 \pm 1.1 \pm 0.5$	$0.2 \pm 0.4 \pm 0.1$	$0.5 \pm 0.7 \pm 0.3$
DY+jets	< 0.1	$0.8 \pm 0.8 \pm 0.1$	< 0.1	< 0.1	< 0.1	$0.1 \pm 0.1 \pm 0.1$
Top quark	$0.3 \pm 0.3 \pm 0.1$	$1.8 \pm 1.2 \pm 0.2$	$1.7 \pm 1.2 \pm 0.6$	$0.2 \pm 0.2 \pm 0.1$	$0.2 \pm 0.2 \pm 0.1$	$1.4 \pm 0.8 \pm 2.0$
Other SM	$0.3 \pm 0.3 \pm 0.1$	$1.4 \pm 0.6 \pm 0.5$	$1.5 \pm 0.6 \pm 0.4$	$0.9 \pm 0.5 \pm 0.4$	$0.6 \pm 0.4 \pm 0.5$	$2.0 \pm 0.7 \pm 1.0$
Total prediction	$2.1 \pm 0.9 \pm 0.4$	$6.4 \pm 1.8 \pm 1.0$	$4.6 \pm 1.6 \pm 0.9$	$4.5 \pm 1.3 \pm 0.8$	$1.0 \pm 0.6 \pm 0.5$	$4.2 \pm 1.3 \pm 1.8$
Observed	1	6	7	5	2	7
Signal	$1.3 \pm 0.4 \pm 0.2$	$0.9 \pm 0.2 \pm 0.1$	$0.7 \pm 0.1 \pm 0.5$	$1.5 \pm 0.4 \pm 0.2$	$0.4 \pm 0.1 \pm 0.1$	$1.0 \pm 0.1 \pm 0.2$

Table 6 Predicted background yields and observed event counts in the most sensitive last bins of the BDT distributions in the $e\tau_h$ and $\mu\tau_h$ final states, in data collected in 2017. The numbers in parentheses in the first row are the $\tilde{\tau}$ and $\tilde{\chi}_1^0$ masses corresponding to the signal model for left-handed $\tilde{\tau}$ pair production that is used to train the BDT. In the bottom row, we list the corresponding predicted signal yields in the last bin of the BDT distribution. The first and second uncertainties given are statistical and systematic, respectively

BDT training	BDT($\mu\tau_h$,100,1)	BDT($\mu\tau_h$,150,1)	BDT($\mu\tau_h$,200,1)	BDT($e\tau_h$,100,1)	BDT($e\tau_h$,150,1)	BDT($e\tau_h$,200,1)
Misidentified τ_h	$0.9 \pm 0.5 \pm 0.4$	< 0.1	< 0.1	$2.5 \pm 0.9 \pm 1.3$	$0.3 \pm 0.3 \pm 0.1$	< 0.1
DY+jets	$2.1 \pm 2.1 \pm 3.3$	< 0.1	< 0.1	< 0.1	< 0.1	< 0.1
Top quark	< 0.1	$0.9 \pm 0.4 \pm 0.8$	$0.6 \pm 0.5 \pm 0.5$	$0.3 \pm 0.3 \pm 0.1$	< 0.1	$0.2 \pm 0.2 \pm 0.2$
Other SM	< 0.1	$1.0 \pm 0.7 \pm 1.6$	$0.6 \pm 0.6 \pm 1.1$	$1.0 \pm 0.7 \pm 1.5$	$0.2 \pm 0.2 \pm 0.5$	$1.0 \pm 0.6 \pm 1.6$
Total prediction	$3.0 \pm 2.2 \pm 3.1$	$2.0 \pm 1.0 \pm 2.0$	$1.2 \pm 0.7 \pm 1.3$	$3.7 \pm 1.1 \pm 2.3$	$0.4 \pm 0.4 \pm 0.5$	$1.2 \pm 0.7 \pm 1.6$
Observed	2	6	2	2	1	1
Signal	$0.6 \pm 0.3 \pm 0.1$	$0.4 \pm 0.1 \pm 0.8$	$0.6 \pm 0.1 \pm 0.3$	$1.0 \pm 0.4 \pm 0.1$	$0.2 \pm 0.1 \pm 0.1$	$0.2 \pm 0.1 \pm 0.1$

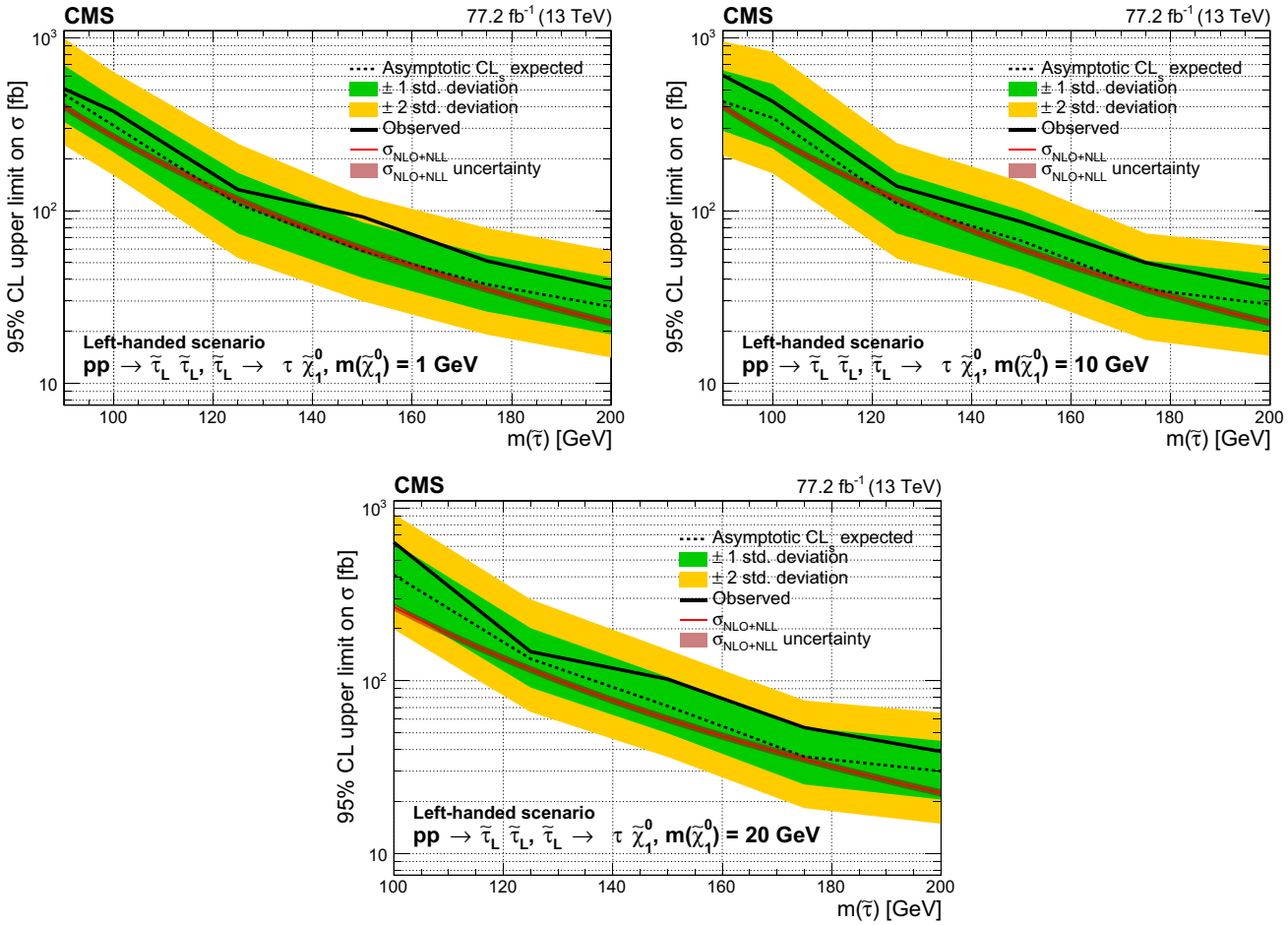

Fig. 8 Upper limit on the cross section (σ) of $\tilde{\tau}$ pair production excluded at 95% CL as a function of the $\tilde{\tau}$ mass in the purely left-handed $\tilde{\tau}$ models for a $\tilde{\chi}_1^0$ mass of 1 GeV (upper left), 10 GeV (upper right) and 20 GeV (lower). The results shown are for the statistical combination of the 2016 and 2017 data in the $\tau_h\tau_h$ and $\ell\tau_h$ analyses. The inner (green) and outer (yellow) bands indicate the respective regions containing 68 and 95% of the distribution of limits expected under the background-only hypothesis. The solid red line indicates the NLO+NLL prediction for the signal production cross section calculated with RESUMMINO [37], while the red shaded band represents the uncertainty in the prediction

modeling. The reweighting factors are obtained from studies of Z boson events. We take the deviation of the reweighting factors from unity as a systematic uncertainty.

The uncertainty in the integrated luminosity is taken into account in all background estimates for which we do not extract normalization scale factors in dedicated data CRs,

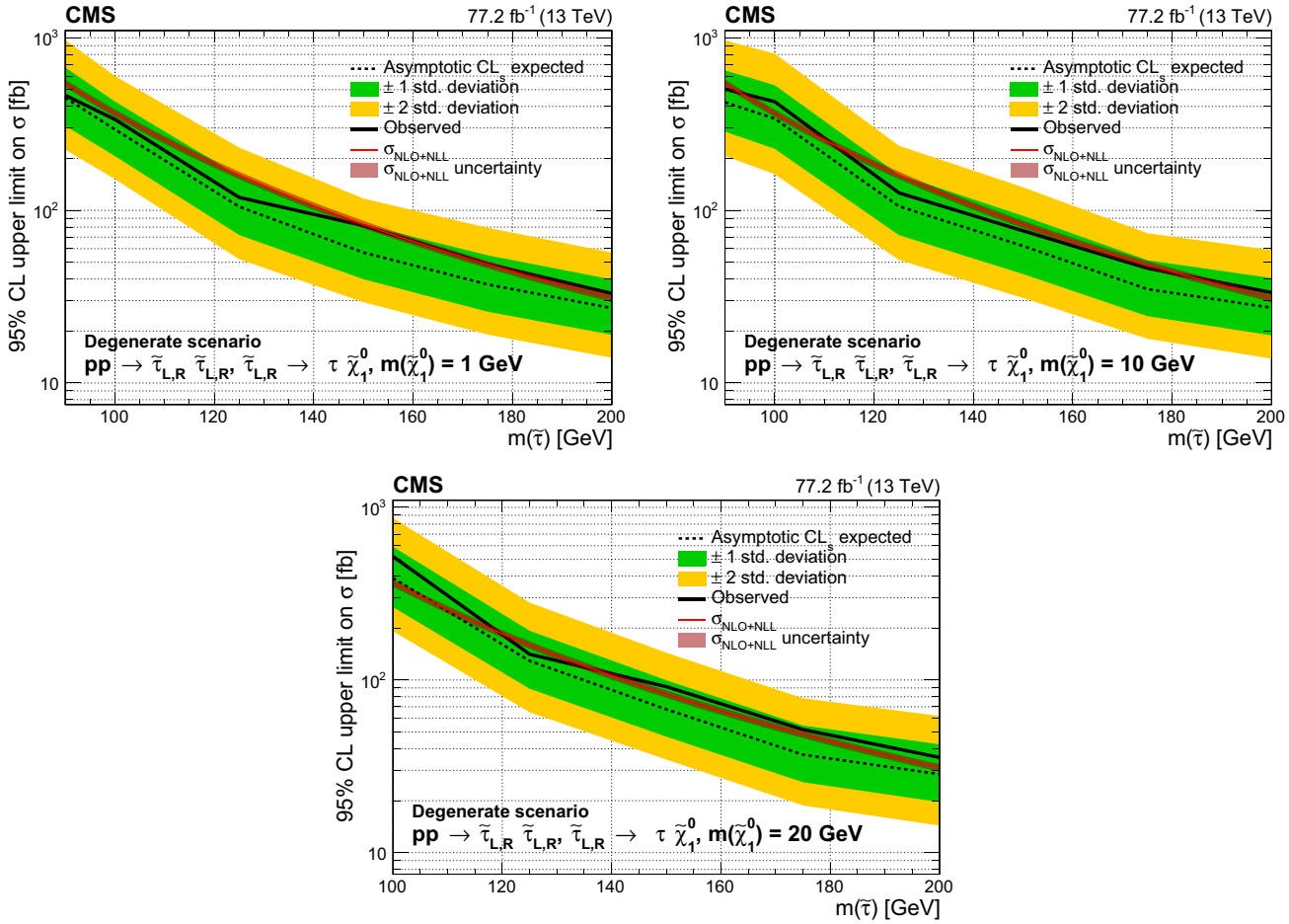

Fig. 9 Upper limit on the cross section (σ) of $\tilde{\tau}$ pair production excluded at 95% CL as a function of the $\tilde{\tau}$ mass in the degenerate $\tilde{\tau}$ models for a $\tilde{\chi}_1^0$ mass of 1 GeV (upper left), 10 GeV (upper right) and 20 GeV (lower). The results shown are for the statistical combination of the 2016 and 2017 data in the $\tau_h\tau_h$ and $\ell\tau_h$ analyses. The inner (green) and outer (yellow) bands indicate the respective regions containing 68 and 95% of the distribution of limits expected under the background-only hypothesis. The solid red line indicates the NLO+NLL prediction for the signal production cross section calculated with RESUMMINO [37], while the red shaded band represents the uncertainty in the prediction

as well as for signal estimates. This uncertainty corresponds to 2.5% [72] and 2.3% [73] for the 2016 and 2017 data, respectively. With the exception of statistical uncertainties, most other uncertainties are of similar size between the 2016 and 2017 analyses. The main systematic uncertainties for signal and background are summarized in Table 2.

In general, we treat all statistical uncertainties as uncorrelated. In addition, all systematic uncertainties arising from statistical limitations in the 2016 and 2017 data are assumed to be uncorrelated while systematic uncertainties from similar sources are treated as correlated or partially correlated across the various background and signal predictions. For the combination of the $\tau_h\tau_h$ and $\ell\tau_h$ analyses, we correlate uncertainties related to object reconstruction, with the exception of the τ_h selection efficiency, which is treated as uncorrelated because of the use of different isolation algorithms.

7 Results and interpretation

The results of the search in the $\tau_h\tau_h$ final state are presented in Fig. 5 and summarized in Tables 3 and 4. The background predictions resulting from a maximum likelihood fit to the data under the background-only hypothesis are shown in the lower row of Fig. 5. The BDT distributions corresponding to a training for a $\tilde{\tau}$ mass of 100 GeV and a $\tilde{\chi}_1^0$ mass of 1 GeV are shown before and after the maximum-likelihood fit to the data in Figs. 6 and 7 for the $\mu\tau_h$ and $e\tau_h$ final states, respectively. The data are consistent with the prediction for SM background. The predicted and observed event yields in the last, most sensitive BDT bins are summarized in Tables 5 and 6 for $\ell\tau_h$ final states. For the statistical interpretation of these results, the normalization uncertainties affecting background and signal predictions are generally assumed to be log-normally distributed. For statistical uncertainties limited

by small event counts in data or simulation, we use a Γ distribution.

The results are used to set upper limits on the cross section for the production of $\widetilde{\tau}$ pairs in the context of simplified models [25–27,74] using all of the exclusive $\tau_h\tau_h$ SRs and the $\ell\tau_h$ BDT distributions in a full statistical combination. The limits are evaluated using likelihood fits with the signal strength, background event yields, and nuisance parameters corresponding to the uncertainties in the signal and background estimates as fitted parameters. The nuisance parameters are constrained within their uncertainties in the fit. We assume that the $\widetilde{\tau}$ decays with 100% branching fraction to a τ lepton and a $\widetilde{\chi}_1^0$. The 95% CL upper limits on SUSY production cross sections are calculated using a modified frequentist approach with the CL_s criterion [75,76]. An asymptotic approximation is used for the test statistic [77,78], $q_\mu = -2\ln\mathcal{L}_\mu/\mathcal{L}_{\max}$, where $\mathcal{L}_{\max}$ is the maximum likelihood determined by allowing all fitted parameters, including the signal strength μ, to vary, and $\mathcal{L}_\mu$ is the maximum likelihood for a fixed signal strength. Figure 8 shows the limits obtained for purely left-handed $\widetilde{\tau}$ pair production, while Fig. 9 shows the limits obtained for the degenerate $\widetilde{\tau}$ model in which both left- and right-handed $\widetilde{\tau}$ pairs are produced. The $\tau_h\tau_h$ analysis makes the dominant contribution to the search sensitivity. A slight excess of events over the background expectation in the $\tau_h\tau_h$ SRs results in an observed limit that is weaker than the expected limit. The strongest limits are observed in the case of a nearly massless $\widetilde{\chi}_1^0$. In general, the constraints are weaker for higher values of the $\widetilde{\chi}_1^0$ mass because of smaller experimental acceptances. For $\widetilde{\tau}$ masses above $\approx$150 GeV, however, the sensitivity does not degrade significantly when the $\widetilde{\chi}_1^0$ mass increases up to 20 GeV. In the purely left-handed model, the strongest limits are observed for a $\widetilde{\tau}$ mass of 125 GeV where we exclude a $\widetilde{\tau}$ pair production cross section of 132 fb. This value is a factor of 1.14 larger than the theoretical cross section. In the degenerate $\widetilde{\tau}$ model we exclude $\widetilde{\tau}$ masses between 90 and 150 GeV under the assumption of a nearly massless $\widetilde{\chi}_1^0$.

8 Summary

A search for direct τ slepton ($\widetilde{\tau}$) pair production has been performed in proton–proton collisions at a center-of-mass energy of 13 TeV in events with a τ lepton pair and significant missing transverse momentum. Search regions are defined using kinematic observables that exploit expected differences in discriminants between signal and background. The data used for this search correspond to an integrated luminosity of 77.2 fb^{-1} collected in 2016 and 2017 with the CMS detector. No excess above the expected standard model background has been observed. Upper limits have been set on the cross section for direct $\widetilde{\tau}$ pair production for simplified models in which each $\widetilde{\tau}$ decays to a τ lepton and the lightest neutralino, with the latter being assumed to be the lightest supersymmetric particle. For purely left-handed $\widetilde{\tau}$ pair production, the analysis is most sensitive to a $\widetilde{\tau}$ mass of 125 GeV when the neutralino is nearly massless. The observed limit is a factor of 1.14 larger than the expected production cross section in this model. The limits observed for left-handed $\widetilde{\tau}$ pair production are the strongest obtained thus far for low values of the $\widetilde{\tau}$ mass. In a more optimistic, degenerate production model, in which both left- and right-handed $\widetilde{\tau}$ pairs are produced, we exclude $\widetilde{\tau}$ masses up to 150 GeV, again under the assumption of a nearly massless neutralino. These results represent the first exclusion reported for this model for low values of the $\widetilde{\tau}$ mass between 90 and 120 GeV.

Acknowledgements We congratulate our colleagues in the CERN accelerator departments for the excellent performance of the LHC and thank the technical and administrative staffs at CERN and at other CMS institutes for their contributions to the success of the CMS effort. In addition, we gratefully acknowledge the computing centers and personnel of the Worldwide LHC Computing Grid for delivering so effectively the computing infrastructure essential to our analyses. Finally, we acknowledge the enduring support for the construction and operation of the LHC and the CMS detector provided by the following funding agencies: BMBWF and FWF (Austria); FNRS and FWO (Belgium); CNPq, CAPES, FAPERJ, FAPERGS, and FAPESP (Brazil); MES (Bulgaria); CERN; CAS, MoST, and NSFC (China); COLCIENCIAS (Colombia); MSES and CSF (Croatia); RPF (Cyprus); SENESCYT (Ecuador); MoER, ERC IUT, PUT and ERDF (Estonia); Academy of Finland, MEC, and HIP (Finland); CEA and CNRS/IN2P3 (France); BMBF, DFG, and HGF (Germany); GSRT (Greece); NKFIA (Hungary); DAE and DST (India); IPM (Iran); SFI (Ireland); INFN (Italy); MSIP and NRF (Republic of Korea); MES (Latvia); LAS (Lithuania); MOE and UM (Malaysia); BUAP, CINVESTAV, CONACYT, LNS, SEP, and UASLP-FAI (Mexico); MOS (Montenegro); MBIE (New Zealand); PAEC (Pakistan); MSHE and NSC (Poland); FCT (Portugal); JINR (Dubna); MON, RosAtom, RAS, RFBR, and NRC KI (Russia); MESTD (Serbia); SEIDI, CPAN, PCTI, and FEDER (Spain); MOSTR (Sri Lanka); Swiss Funding Agencies (Switzerland); MST (Taipei); ThEPCenter, IPST, STAR, and NSTDA (Thailand); TUBITAK and TAEK (Turkey); NASU and SFFR (Ukraine); STFC (UK); DOE and NSF (USA). Individuals have received support from the Marie-Curie program and the European Research Council and Horizon 2020 Grant, contract Nos. 675440, 752730, and 765710 (European Union); the Leventis Foundation; the A.P. Sloan Foundation; the Alexander von Humboldt Foundation; the Belgian Federal Science Policy Office; the Fonds pour la Formation à la Recherche dans l'Industrie et dans l'Agriculture (FRIA-Belgium); the Agentschap voor Innovatie door Wetenschap en Technologie (IWT-Belgium); the F.R.S.-FNRS and FWO (Belgium) under the "Excellence of Science – EOS" – be.h project n. 30820817; the Beijing Municipal Science & Technology Commission, No. Z181100004218003; the Ministry of Education, Youth and Sports (MEYS) of the Czech Republic; the Lendület ("Momentum") Program and the János Bolyai Research Scholarship of the Hungarian Academy of Sciences, the New National Excellence Program ÚNKP, the NKFIA research grants 123842, 123959, 124845, 124850, 125105, 128713, 128786, and 129058 (Hungary); the Council of Science and Industrial Research, India; the HOMING PLUS program of the Foundation for Polish Science, cofinanced from European Union, Regional Development Fund, the Mobility Plus program of the Ministry of Science and Higher Education, the National Science Center (Poland), contracts Harmonia 2014/14/M/ST2/00428, Opus 2014/13/B/ST2/02543,

2014/15/B/ST2/03998, and 2015/19/B/ST2/02861, Sonata-bis 2012/07/E/ST2/01406; the National Priorities Research Program by Qatar National Research Fund; the Ministry of Science and Education, grant no. 3.2989.2017 (Russia); the Programa Estatal de Fomento de la Investigación Científica y Técnica de Excelencia María de Maeztu, grant MDM-2015-0509 and the Programa Severo Ochoa del Principado de Asturias; the Thalis and Aristeia programs cofinanced by EU-ESF and the Greek NSRF; the Rachadapisek Sompot Fund for Postdoctoral Fellowship, Chulalongkorn University and the Chulalongkorn Academic into Its 2nd Century Project Advancement Project (Thailand); the Welch Foundation, contract C-1845; and the Weston Havens Foundation (USA).

Data Availability Statement This manuscript has no associated data or the data will not be deposited. [Authors' comment: Release and preservation of data used by the CMS Collaboration as the basis for publications is guided by the CMS policy as written in its document "CMS data preservation, re-use and open access policy" (https://cms-docdb.cern.ch/cgi-bin/PublicDocDB/RetrieveFile?docid=6032&filename=CMSDataPolicyV1.2.pdf&version=2).]

Funded by SCOAP[3].

References

1. P. Ramond, Dual theory for free fermions. Phys. Rev. D **3**, 2415 (1971). https://doi.org/10.1103/PhysRevD.3.2415
2. Y.A. Gol'fand, E.P. Likhtman, Extension of the algebra of Poincaré group generators and violation of P invariance. JETP Lett. **13**, 323 (1971). http://www.jetpletters.ac.ru/ps/1584/article_24309.pdf
3. A. Neveu, J.H. Schwarz, Factorizable dual model of pions. Nucl. Phys. B **31**, 86 (1971). https://doi.org/10.1016/0550-3213(71)90448-2
4. D.V. Volkov, V.P. Akulov, Possible universal neutrino interaction. JETP Lett. **16**, 438 (1972)
5. J. Wess, B. Zumino, A Lagrangian model invariant under supergauge transformations. Phys. Lett. B **49**, 52 (1974). https://doi.org/10.1016/0370-2693(74)90578-4
6. J. Wess, B. Zumino, Supergauge transformations in four dimensions. Nucl. Phys. B **70**, 39 (1974). https://doi.org/10.1016/0550-3213(74)90355-1
7. P. Fayet, Supergauge invariant extension of the Higgs mechanism and a model for the electron and its neutrino. Nucl. Phys. B **90**, 104 (1975). https://doi.org/10.1016/0550-3213(75)90636-7
8. H.P. Nilles, Supersymmetry, supergravity and particle physics. Phys. Rep. **110**, 1 (1984). https://doi.org/10.1016/0370-1573(84)90008-5
9. E. Gildener, Gauge symmetry hierarchies. Phys. Rev. D **14**, 1667 (1976). https://doi.org/10.1103/PhysRevD.14.1667
10. M.J.G. Veltman, Second threshold in weak interactions. Acta Phys. Polon. B **8**, 475 (1977)
11. G. 't Hooft, Naturalness, chiral symmetry, and spontaneous chiral symmetry breaking. NATO Sci. Ser. B **59**, 135 (1980)
12. E. Witten, Dynamical breaking of supersymmetry. Nucl. Phys. B **188**, 513 (1981). https://doi.org/10.1016/0550-3213(81)90006-7
13. G.R. Farrar, P. Fayet, Phenomenology of the production, decay, and detection of new hadronic states associated with supersymmetry. Phys. Lett. B **76**, 575 (1978). https://doi.org/10.1016/0370-2693(78)90858-4
14. H. Goldberg, Constraint on the Photino Mass from Cosmology. Phys. Rev. Lett. **50**, 1419 (1983). https://doi.org/10.1103/PhysRevLett.50.1419. [Erratum: Phys. Rev. Lett.103,099905(2009)]
15. J.R. Ellis et al., Supersymmetric relics from the big bang. Nucl. Phys. B **238**, 453–476 (1984). https://doi.org/10.1016/0550-3213(84)90461-9. [223(1983)]
16. G. Jungman, M. Kamionkowski, K. Griest, Supersymmetric dark matter. Phys. Rept. **267**, 195 (1996). https://doi.org/10.1016/0370-1573(95)00058-5. arXiv:hep-ph/9506380
17. G. Hinshaw et al., Nine-year Wilkinson microwave anisotropy probe (WMAP) observations: cosmological parameter results. Astrophys. J. Suppl. **208**, 19 (2013). https://doi.org/10.1088/0067-0049/208/2/19. arXiv:1212.5226
18. K. Griest, D. Seckel, Three exceptions in the calculation of relic abundances. Phys. Rev. D **43**, 3191 (1991). https://doi.org/10.1103/PhysRevD.43.3191
19. D.A. Vasquez, G. Bélanger, C. Boehm, Revisiting light neutralino scenarios in the MSSM. Phys. Rev. D **84**, 095015 (2011). https://doi.org/10.1103/PhysRevD.84.095015. arXiv:1108.1338
20. S.F. King, J.P. Roberts, D.P. Roy, Natural dark matter in SUSY GUTs with non-universal gaugino masses. JHEP **10**, 106 (2007). https://doi.org/10.1088/1126-6708/2007/10/106. arXiv:0705.4219
21. M. Battaglia et al., Proposed post-LEP benchmarks for supersymmetry. Eur. Phys. J. C **22**, 535 (2001). https://doi.org/10.1007/s100520100792. arXiv:hep-ph/0106204
22. R.L. Arnowitt et al., Determining the dark matter relic density in the minimal supergravity stau-neutralino coannihilation region at the Large Hadron Collider. Phys. Rev. Lett. **100**, 231802 (2008). https://doi.org/10.1103/PhysRevLett.100.231802. arXiv:0802.2968
23. G. Bélanger, S. Biswas, C. Boehm, B. Mukhopadhyaya, Light neutralino dark matter in the MSSM and its implication for LHC searches for staus. JHEP **12**, 076 (2012). https://doi.org/10.1007/JHEP12(2012)076. arXiv:1206.5404
24. E. Arganda, V. Martin-Lozano, A.D. Medina, N. Mileo, Potential discovery of staus through heavy Higgs boson decays at the LHC. JHEP **09**, 056 (2018). https://doi.org/10.1007/JHEP09(2018)056. arXiv:1804.10698
25. J. Alwall, P. Schuster, N. Toro, Simplified models for a first characterization of new physics at the LHC. Phys. Rev. D **79**, 075020 (2009). https://doi.org/10.1103/PhysRevD.79.075020. arXiv:0810.3921
26. J. Alwall, M.-P. Le, M. Lisanti, J. Wacker, Model-independent jets plus missing energy searches. Phys. Rev. D **79**, 015005 (2009). https://doi.org/10.1103/PhysRevD.79.015005. arXiv:0809.3264
27. LHC New Physics Working Group, Simplified models for LHC new physics searches. J. Phys. G **39**, 105005 (2012). https://doi.org/10.1088/0954-3899/39/10/105005. arXiv:1105.2838
28. ALEPH Collaboration, Search for scalar leptons in e^+e^- collisions at center-of-mass energies up to 209 GeV. Phys. Lett. B **526**, 206 (2002). https://doi.org/10.1016/S0370-2693(01)01494-0. arXiv:hep-ex/0112011
29. DELPHI Collaboration, Searches for supersymmetric particles in e^+e^- collisions up to 208 GeV and interpretation of the results within the MSSM. Eur. Phys. J. C **31**, 421 (2003). https://doi.org/10.1140/epjc/s2003-01355-5. arXiv:hep-ex/0311019

30. L3 Collaboration, Search for scalar leptons and scalar quarks at LEP. Phys. Lett. B **580**, 37 (2004). https://doi.org/10.1016/j.physletb.2003.10.010. arXiv:hep-ex/0310007
31. OPAL Collaboration, Search for anomalous production of dilepton events with missing transverse momentum in e^+e^- collisions at $\sqrt{s}$ = 183 GeV to 209 GeV. Eur. Phys. J. C **32**, 453 (2004). https://doi.org/10.1140/epjc/s2003-01466-y. arXiv:hep-ex/0309014
32. ATLAS Collaboration, Search for the direct production of charginos, neutralinos and staus in final states with at least two hadronically decaying taus and missing transverse momentum in pp collisions at $\sqrt{s}$ = 8 TeV with the ATLAS detector. *JHEP* **10**, 96 (2014). https://doi.org/10.1007/JHEP10(2014)096, arXiv:1407.0350
33. ATLAS Collaboration, Search for the electroweak production of supersymmetric particles in $\sqrt{s}$ = 8 TeV pp collisions with the ATLAS detector. Phys. Rev. D **93**, 052002 (2016). https://doi.org/10.1103/PhysRevD.93.052002. arXiv:1509.07152
34. CMS Collaboration, Search for electroweak production of charginos in final states with two tau leptons in pp collisions at $\sqrt{s}$ = 8 TeV. JHEP **04**, 018 (2017). https://doi.org/10.1007/JHEP04(2017)018. arXiv:1610.04870
35. CMS Collaboration, Search for supersymmetry in events with a τ lepton pair and missing transverse momentum in proton-proton collisions at $\sqrt{s}$ = 13 TeV. JHEP **11**, 151 (2018). https://doi.org/10.1007/JHEP11(2018)151. arXiv:1807.02048
36. GEANT4 Collaboration, GEANT4—a simulation toolkit. Nucl. Instrum. Meth. A **506**, 250 (2003). https://doi.org/10.1016/S0168-9002(03)01368-8
37. B. Fuks, M. Klasen, D.R. Lamprea, M. Rothering, Revisiting slepton pair production at the Large Hadron Collider. JHEP **01**, 168 (2014). https://doi.org/10.1007/JHEP01(2014)168. arXiv:1310.2621
38. CMS Collaboration, The CMS trigger system. JINST **12**, P01020 (2017). https://doi.org/10.1088/1748-0221/12/01/P01020. arXiv:1609.02366
39. CMS Collaboration, The CMS experiment at the CERN LHC. JINST **3**, S08004 (2008). https://doi.org/10.1088/1748-0221/3/08/S08004
40. CMS Collaboration, Particle-flow reconstruction and global event description with the CMS detector. JINST **12**, P10003 (2017). https://doi.org/10.1088/1748-0221/12/10/P10003. arXiv:1706.04965
41. CMS Collaboration, Performance of missing transverse momentum reconstruction in proton-proton collisions at $\sqrt{s}$ = 13 TeV using the CMS detector. JINST **14**, P07004 (2019). https://doi.org/10.1088/1748-0221/14/07/P07004. arXiv:1903.06078
42. M. Cacciari, G.P. Salam, G. Soyez, The anti-k_T jet clustering algorithm. JHEP **04**, 063 (2008). https://doi.org/10.1088/1126-6708/2008/04/063. arXiv:0802.1189
43. M. Cacciari, G.P. Salam, G. Soyez, FastJet user manual. Eur. Phys. J. C **72**, 1896 (2012). https://doi.org/10.1140/epjc/s10052-012-1896-2. arXiv:1111.6097
44. CMS Collaboration, Study of pileup removal algorithms for jets. CMS Physics Analysis Summary CMS-PAS-JME-14-001, 2014. https://cds.cern.ch/record/1751454
45. CMS Collaboration, Identification of heavy-flavour jets with the CMS detector in pp collisions at 13 TeV. JINST **13**, P05011 (2018). https://doi.org/10.1088/1748-0221/13/05/P05011. arXiv:1712.07158
46. CMS Collaboration, Performance of electron reconstruction and selection with the CMS detector in proton-proton collisions at $\sqrt{s}$ = 8 TeV. JINST **10**, P06005 (2015). https://doi.org/10.1088/1748-0221/10/06/P06005. arXiv:1502.02701
47. CMS Collaboration, Performance of the CMS muon detector and muon reconstruction with proton-proton collisions at $\sqrt{s}$ = 13 TeV. JINST **13**, P06015 (2018). https://doi.org/10.1088/1748-0221/13/06/P06015. arXiv:1804.04528
48. CMS Collaboration, Performance of reconstruction and identification of τ leptons decaying to hadrons and ν_τ in pp collisions at $\sqrt{s}$ = 13 TeV. JINST **13**, P10005 (2018). https://doi.org/10.1088/1748-0221/13/10/P10005. arXiv:1809.02816
49. Y. Lecun, L. Bottou, Y. Bengio, P. Haffner, Gradient-based learning applied to document recognition. in *Proceedings of the IEEE*, p. 2278. (1998). https://doi.org/10.1109/5.726791
50. J. Alwall et al., The automated computation of tree-level and next-to-leading order differential cross sections, and their matching to parton shower simulations. JHEP **07**, 079 (2014). https://doi.org/10.1007/JHEP07(2014)079. arXiv:1405.0301
51. P. Nason, A new method for combining NLO QCD with shower Monte Carlo algorithms. JHEP **11**, 040 (2004). https://doi.org/10.1088/1126-6708/2004/11/040. arXiv:hep-ph/0409146
52. S. Frixione, P. Nason, C. Oleari, Matching NLO QCD computations with parton shower simulations: the POWHEG method. JHEP **11**, 070 (2007). https://doi.org/10.1088/1126-6708/2007/11/070. arXiv:0709.2092
53. S. Alioli, P. Nason, C. Oleari, E. Re, A general framework for implementing NLO calculations in shower Monte Carlo programs: the POWHEG BOX. JHEP **06**, 043 (2010). https://doi.org/10.1007/JHEP06(2010)043. arXiv:1002.2581
54. E. Re, Single-top Wt-channel production matched with parton showers using the POWHEG method. Eur. Phys. J. C **71**, 1547 (2011). https://doi.org/10.1140/epjc/s10052-011-1547-z. arXiv:1009.2450
55. T. Sjöstrand et al., An introduction to PYTHIA 8.2. Comput. Phys. Commun. **191**, 159 (2015). https://doi.org/10.1016/j.cpc.2015.01.024. arXiv:1410.3012
56. A. Kalogeropoulos, J. Alwall, The SysCalc code: A tool to derive theoretical systematic uncertainties. (2018). arXiv:1801.08401
57. CMS Collaboration, Event generator tunes obtained from underlying event and multiparton scattering measurements. Eur. Phys. J. C **76**, 155 (2016). https://doi.org/10.1140/epjc/s10052-016-3988-x. arXiv:1512.00815
58. CMS Collaboration, Investigations of the impact of the parton shower tuning in Pythia 8 in the modelling of $t\bar{t}$ at $\sqrt{s}$ = 8 and 13 TeV. CMS Physics Analysis Summary CMS-PAS-TOP-16-021, (2016). https://cds.cern.ch/record/2235192
59. CMS Collaboration, Extraction and validation of a new set of CMS PYTHIA8 tunes from underlying-event measurements. Eur. Phys. J. C **80**, 4 (2020). https://doi.org/10.1140/epjc/s10052-019-7499-4
60. NNPDF Collaboration, Parton distributions for the LHC Run II. *JHEP* **04** 040, (2015). https://doi.org/10.1007/JHEP04(2015)040, arXiv:1410.8849
61. CMS Collaboration, Search for top-squark pair production in the single-lepton final state in pp collisions at $\sqrt{s}$ = 8 TeV. Eur. Phys. J. C **73**, 2677 (2013). https://doi.org/10.1140/epjc/s10052-013-2677-2. arXiv:1308.1586
62. C.G. Lester, D.J. Summers, Measuring masses of semi-invisibly decaying particle pairs produced at hadron colliders. Phys. Lett. B **463**, 99 (1999). https://doi.org/10.1016/S0370-2693(99)00945-4. arXiv:hep-ph/9906349
63. A. Barr, C. Lester, P. Stephens, m_{T2}: the truth behind the glamour. J. Phys. G **29**, 2343 (2003). https://doi.org/10.1088/0954-3899/29/10/304. arXiv:hep-ph/0304226
64. C.G. Lester, B. Nachman, Bisection-based asymmetric m_{T2} computation: a higher precision calculator than existing symmetric methods. JHEP **03**, 100 (2015). https://doi.org/10.1007/JHEP03(2015)100. arXiv:1411.4312
65. D. Tovey, On measuring the masses of pair-produced semi-invisibly decaying particles at hadron colliders. JHEP **04**, 034 (2008). https://doi.org/10.1088/1126-6708/2008/04/034. arXiv:0802.2879

66. G. Polesello, D. Tovey, Supersymmetric particle mass measurement with boost-corrected contransverse mass. JHEP **03**, 030 (2010). https://doi.org/10.1007/JHEP03(2010)030. arXiv:0910.0174
67. C. Cuenca Almenar, Search for the neutral MSSM Higgs bosons in the ditau decay channels at CDF Run II. PhD thesis, Valencia U., IFIC, (2008). https://doi.org/10.2172/953708
68. CMS Collaboration, Search for neutral MSSM Higgs bosons decaying to a pair of tau leptons in pp collisions. JHEP **10**, 160 (2014). https://doi.org/10.1007/JHEP10(2014)160. arXiv:1408.3316
69. L. Demortier, P values and nuisance parameters. in *Statistical issues for LHC physics. Proceedings, Workshop, PHYSTAT-LHC, Geneva, Switzerland, June 27–29, 2007*, p. 23. (2008). https://doi.org/10.5170/CERN-2008-001
70. CMS Collaboration, Measurement of the differential Drell–Yan cross section in proton–proton collisions at $\sqrt{s} = 13$ TeV. JHEP **12**, 059 (2019). https://doi.org/10.1007/JHEP12(2019)059
71. CMS Collaboration, Measurements of $t\bar{t}$ differential cross sections in proton-proton collisions at $\sqrt{s} = 13$ TeV using events containing two leptons. JHEP **02**, 149 (2019). https://doi.org/10.1007/JHEP02(2019)149. arXiv:1811.06625
72. CMS Collaboration, CMS luminosity measurements for the 2016 data taking period. CMS Physics Analysis Summary CMS-PAS-LUM-17-001, 2017. http://cds.cern.ch/record/2257069
73. CMS Collaboration, CMS luminosity measurement for the 2017 data-taking period at $\sqrt{s} = 13$ TeV. CMS Physics Analysis Summary CMS-PAS-LUM-17-004, 2018. http://cds.cern.ch/record/2621960
74. CMS Collaboration, Interpretation of searches for supersymmetry with simplified models. Phys. Rev. D **88**, 052017 (2013). https://doi.org/10.1103/PhysRevD.88.052017. arXiv:1301.2175
75. T. Junk, Confidence level computation for combining searches with small statistics. Nucl. Instrum. Meth. A **434**, 435 (1999). https://doi.org/10.1016/S0168-9002(99)00498-2. arXiv:hep-ex/9902006
76. A.L. Read, Presentation of search results: the CL_s technique. J. Phys. G **28**, 2693 (2002). https://doi.org/10.1088/0954-3899/28/10/313
77. The ATLAS Collaboration, The CMS Collaboration, The LHC Higgs Combination Group, Procedure for the LHC Higgs boson search combination in Summer 2011. Technical Report CMS-NOTE-2011-005, ATL-PHYS-PUB-2011-11, (2011). https://cds.cern.ch/record/1379837
78. G. Cowan, K. Cranmer, E. Gross, O. Vitells, Asymptotic formulae for likelihood-based tests of new physics. Eur. Phys. J. C **71**, 1554 (2011). https://doi.org/10.1140/epjc/s10052-011-1554-0. arXiv:1007.1727. [Erratum: 10.1140/epjc/s10052-013-2501-z]

CMS Collaboration

Yerevan Physics Institute, Yerevan, Armenia
A. M. Sirunyan[†], A. Tumasyan

Institut für Hochenergiephysik, Wien, Austria
W. Adam, F. Ambrogi, T. Bergauer, J. Brandstetter, M. Dragicevic, J. Erö, A. Escalante Del Valle, M. Flechl, R. Frühwirth[1], M. Jeitler[1], N. Krammer, I. Krätschmer, D. Liko, T. Madlener, I. Mikulec, N. Rad, J. Schieck[1], R. Schöfbeck, M. Spanring, D. Spitzbart, W. Waltenberger, C.-E. Wulz[1], M. Zarucki

Institute for Nuclear Problems, Minsk, Belarus
V. Drugakov, V. Mossolov, J. Suarez Gonzalez

Universiteit Antwerpen, Antwerpen, Belgium
M. R. Darwish, E. A. De Wolf, D. Di Croce, X. Janssen, A. Lelek, M. Pieters, H. Rejeb Sfar, H. Van Haevermaet, P. Van Mechelen, S. Van Putte, N. Van Remortel

Vrije Universiteit Brussel, Brussel, Belgium
F. Blekman, E. S. Bols, S. S. Chhibra, J. D'Hondt, J. De Clercq, D. Lontkovskyi, S. Lowette, I. Marchesini, S. Moortgat, L. Moreels, Q. Python, K. Skovpen, S. Tavernier, W. Van Doninck, P. Van Mulders, I. Van Parijs

Université Libre de Bruxelles, Bruxelles, Belgium
D. Beghin, B. Bilin, H. Brun, B. Clerbaux, G. De Lentdecker, H. Delannoy, B. Dorney, L. Favart, A. Grebenyuk, A. K. Kalsi, A. Popov, N. Postiau, E. Starling, L. Thomas, C. Vander Velde, P. Vanlaer, D. Vannerom

Ghent University, Ghent, Belgium
T. Cornelis, D. Dobur, I. Khvastunov[2], M. Niedziela, C. Roskas, D. Trocino, M. Tytgat, W. Verbeke, B. Vermassen, M. Vit, N. Zaganidis

Université Catholique de Louvain, Louvain-la-Neuve, Belgium
O. Bondu, G. Bruno, C. Caputo, P. David, C. Delaere, M. Delcourt, A. Giammanco, V. Lemaitre, A. Magitteri, J. Prisciandaro, A. Saggio, M. Vidal Marono, P. Vischia, J. Zobec

Centro Brasileiro de Pesquisas Fisicas, Rio de Janeiro, Brazil
F. L. Alves, G. A. Alves, G. Correia Silva, C. Hensel, A. Moraes, P. Rebello Teles

Universidade do Estado do Rio de Janeiro, Rio de Janeiro, Brazil
E. Belchior Batista Das Chagas, W. Carvalho, J. Chinellato[3], E. Coelho, E. M. Da Costa, G. G. Da Silveira[4], D. De Jesus Damiao, C. De Oliveira Martins, S. Fonseca De Souza, L. M. Huertas Guativa, H. Malbouisson, J. Martins[5], D. Matos Figueiredo, M. Medina Jaime[6], M. Melo De Almeida, C. Mora Herrera, L. Mundim, H. Nogima, W. L. Prado Da Silva, L. J. Sanchez Rosas, A. Santoro, A. Sznajder, M. Thiel, E. J. Tonelli Manganote[3], F. Torres Da Silva De Araujo, A. Vilela Pereira

Universidade Estadual Paulista[a], Universidade Federal do ABC[b], São Paulo, Brazil
C. A. Bernardes[a], L. Calligaris[a], T. R. Fernandez Perez Tomei[a], E. M. Gregores[b], D. S. Lemos, P. G. Mercadante[b], S. F. Novaes[a], SandraS. Padula[a]

Institute for Nuclear Research and Nuclear Energy, Bulgarian Academy of Sciences, Sofia, Bulgaria
A. Aleksandrov, G. Antchev, R. Hadjiiska, P. Iaydjiev, A. Marinov, M. Misheva, M. Rodozov, M. Shopova, G. Sultanov

University of Sofia, Sofia, Bulgaria
M. Bonchev, A. Dimitrov, T. Ivanov, L. Litov, B. Pavlov, P. Petkov

Beihang University, Beijing, China
W. Fang[7], X. Gao[7], L. Yuan

Institute of High Energy Physics, Beijing, China
M. Ahmad, G. M. Chen, H. S. Chen, M. Chen, C. H. Jiang, D. Leggat, H. Liao, Z. Liu, S. M. Shaheen[8], A. Spiezia, J. Tao, E. Yazgan, H. Zhang, S. Zhang[8], J. Zhao

State Key Laboratory of Nuclear Physics and Technology, Peking University, Beijing, China
A. Agapitos, Y. Ban, G. Chen, A. Levin, J. Li, L. Li, Q. Li, Y. Mao, S. J. Qian, D. Wang, Q. Wang

Tsinghua University, Beijing, China
Z. Hu, Y. Wang

Universidad de Los Andes, Bogota, Colombia
C. Avila, A. Cabrera, L. F. Chaparro Sierra, C. Florez, C. F. González Hernández, M. A. Segura Delgado

Universidad de Antioquia, Medellin, Colombia
J. Mejia Guisao, J. D. Ruiz Alvarez, C. A. Salazar González, N. Vanegas Arbelaez

University of Split, Faculty of Electrical Engineering, Mechanical Engineering and Naval Architecture, Split, Croatia
D. Giljanović, N. Godinovic, D. Lelas, I. Puljak, T. Sculac

University of Split, Faculty of Science, Split, Croatia
Z. Antunovic, M. Kovac

Institute Rudjer Boskovic, Zagreb, Croatia
V. Brigljevic, S. Ceci, D. Ferencek, K. Kadija, B. Mesic, M. Roguljic, A. Starodumov[9], T. Susa

University of Cyprus, Nicosia, Cyprus
M. W. Ather, A. Attikis, E. Erodotou, A. Ioannou, M. Kolosova, S. Konstantinou, G. Mavromanolakis, J. Mousa, C. Nicolaou, F. Ptochos, P. A. Razis, H. Rykaczewski, D. Tsiakkouri

Charles University, Prague, Czech Republic
M. Finger[10], M. Finger Jr.[10], A. Kveton, J. Tomsa

Escuela Politecnica Nacional, Quito, Ecuador
E. Ayala

Universidad San Francisco de Quito, Quito, Ecuador
E. Carrera Jarrin

Academy of Scientific Research and Technology of the Arab Republic of Egypt, Egyptian Network of High Energy Physics, Cairo, Egypt
S. Abu Zeid[11], S. Khalil[12]

National Institute of Chemical Physics and Biophysics, Tallinn, Estonia
S. Bhowmik, A. Carvalho Antunes De Oliveira, R. K. Dewanjee, K. Ehataht, M. Kadastik, M. Raidal, C. Veelken

Department of Physics, University of Helsinki, Helsinki, Finland
P. Eerola, L. Forthomme, H. Kirschenmann, K. Osterberg, M. Voutilainen

Helsinki Institute of Physics, Helsinki, Finland
F. Garcia, J. Havukainen, J. K. Heikkilä, T. Järvinen, V. Karimäki, R. Kinnunen, T. Lampén, K. Lassila-Perini, S. Laurila, S. Lehti, T. Lindén, P. Luukka, T. Mäenpää, H. Siikonen, E. Tuominen, J. Tuominiemi

Lappeenranta University of Technology, Lappeenranta, Finland
T. Tuuva

IRFU, CEA, Université Paris-Saclay, Gif-sur-Yvette, France
M. Besancon, F. Couderc, M. Dejardin, D. Denegri, B. Fabbro, J. L. Faure, F. Ferri, S. Ganjour, A. Givernaud, P. Gras, G. Hamel de Monchenault, P. Jarry, C. Leloup, E. Locci, J. Malcles, J. Rander, A. Rosowsky, M. Ö. Sahin, A. Savoy-Navarro[13], M. Titov

Laboratoire Leprince-Ringuet, CNRS/IN2P3, Ecole Polytechnique, Institut Polytechnique de Paris, Palaiseau, France
S. Ahuja, C. Amendola, F. Beaudette, P. Busson, C. Charlot, B. Diab, G. Falmagne, R. Granier de Cassagnac, I. Kucher, A. Lobanov, C. Martin Perez, M. Nguyen, C. Ochando, P. Paganini, J. Rembser, R. Salerno, J. B. Sauvan, Y. Sirois, A. Zabi, A. Zghiche

Université de Strasbourg, CNRS, IPHC UMR 7178, Strasbourg, France
J.-L. Agram[14], J. Andrea, D. Bloch, G. Bourgatte, J.-M. Brom, E. C. Chabert, C. Collard, E. Conte[14], J.-C. Fontaine[14], D. Gelé, U. Goerlach, M. Jansová, A.-C. Le Bihan, N. Tonon, P. Van Hove

Centre de Calcul de l'Institut National de Physique Nucleaire et de Physique des Particules, CNRS/IN2P3, Villeurbanne, France
S. Gadrat

Université de Lyon, Université Claude Bernard Lyon 1, CNRS-IN2P3, Institut de Physique Nucléaire de Lyon, Villeurbanne, France
S. Beauceron, C. Bernet, G. Boudoul, C. Camen, N. Chanon, R. Chierici, D. Contardo, P. Depasse, H. El Mamouni, J. Fay, S. Gascon, M. Gouzevitch, B. Ille, Sa. Jain, F. Lagarde, I. B. Laktineh, H. Lattaud, M. Lethuillier, L. Mirabito, S. Perries, V. Sordini, G. Touquet, M. Vander Donckt, S. Viret

Georgian Technical University, Tbilisi, Georgia
A. Khvedelidze[10]

Tbilisi State University, Tbilisi, Georgia
Z. Tsamalaidze[10]

RWTH Aachen University, I. Physikalisches Institut, Aachen, Germany
C. Autermann, L. Feld, M. K. Kiesel, K. Klein, M. Lipinski, D. Meuser, A. Pauls, M. Preuten, M. P. Rauch, C. Schomakers, J. Schulz, M. Teroerde, B. Wittmer

RWTH Aachen University, III. Physikalisches Institut A, Aachen, Germany
A. Albert, M. Erdmann, S. Erdweg, T. Esch, B. Fischer, R. Fischer, S. Ghosh, T. Hebbeker, K. Hoepfner, H. Keller, L. Mastrolorenzo, M. Merschmeyer, A. Meyer, P. Millet, G. Mocellin, S. Mondal, S. Mukherjee, D. Noll, A. Novak, T. Pook, A. Pozdnyakov, T. Quast, M. Radziej, Y. Rath, H. Reithler, M. Rieger, J. Roemer, A. Schmidt, S. C. Schuler, A. Sharma, S. Thüer, S. Wiedenbeck

RWTH Aachen University, III. Physikalisches Institut B, Aachen, Germany
G. Flügge, W. Haj Ahmad[15], O. Hlushchenko, T. Kress, T. Müller, A. Nehrkorn, A. Nowack, C. Pistone, O. Pooth, D. Roy, H. Sert, A. Stahl[16]

Deutsches Elektronen-Synchrotron, Hamburg, Germany
M. Aldaya Martin, P. Asmuss, I. Babounikau, H. Bakhshiansohi, K. Beernaert, O. Behnke, U. Behrens,

A. Bermúdez Martínez, D. Bertsche, A. A. Bin Anuar, K. Borras[17], V. Botta, A. Campbell, A. Cardini, P. Connor, S. Consuegra Rodríguez, C. Contreras-Campana, V. Danilov, A. De Wit, M. M. Defranchis, L. Didukh, C. Diez Pardos, D. Domínguez Damiani, G. Eckerlin, D. Eckstein, T. Eichhorn, A. Elwood, E. Eren, E. Gallo[18], A. Geiser, J. M. Grados Luyando, A. Grohsjean, M. Guthoff, M. Haranko, A. Harb, A. Jafari, N. Z. Jomhari, H. Jung, A. Kasem[17], M. Kasemann, H. Kaveh, J. Keaveney, C. Kleinwort, J. Knolle, D. Krücker, W. Lange, T. Lenz, J. Leonard, J. Lidrych, K. Lipka, W. Lohmann[19], R. Mankel, I.-A. Melzer-Pellmann, A. B. Meyer, M. Meyer, M. Missiroli, G. Mittag, J. Mnich, A. Mussgiller, V. Myronenko, D. Pérez Adán, S. K. Pflitsch, D. Pitzl, A. Raspereza, A. Saibel, M. Savitskyi, V. Scheurer, P. Schütze, C. Schwanenberger, R. Shevchenko, A. Singh, H. Tholen, O. Turkot, A. Vagnerini, M. Van De Klundert, G. P. Van Onsem, R. Walsh, Y. Wen, K. Wichmann, C. Wissing, O. Zenaiev, R. Zlebcik

University of Hamburg, Hamburg, Germany
R. Aggleton, S. Bein, L. Benato, A. Benecke, V. Blobel, T. Dreyer, A. Ebrahimi, A. Fröhlich, C. Garbers, E. Garutti, D. Gonzalez, P. Gunnellini, J. Haller, A. Hinzmann, A. Karavdina, G. Kasieczka, R. Klanner, R. Kogler, N. Kovalchuk, S. Kurz, V. Kutzner, J. Lange, T. Lange, A. Malara, J. Multhaup, C. E. N. Niemeyer, A. Perieanu, A. Reimers, O. Rieger, C. Scharf, P. Schleper, S. Schumann, J. Schwandt, J. Sonneveld, H. Stadie, G. Steinbrück, F. M. Stober, M. Stöver, B. Vormwald, I. Zoi

Karlsruher Institut fuer Technologie, Karlsruhe, Germany
M. Akbiyik, C. Barth, M. Baselga, S. Baur, T. Berger, E. Butz, R. Caspart, T. Chwalek, W. De Boer, A. Dierlamm, K. El Morabit, N. Faltermann, M. Giffels, P. Goldenzweig, A. Gottmann, M. A. Harrendorf, F. Hartmann[16], U. Husemann, S. Kudella, S. Mitra, M. U. Mozer, Th. Müller, M. Musich, A. Nürnberg, G. Quast, K. Rabbertz, M. Schröder, I. Shvetsov, H. J. Simonis, R. Ulrich, M. Weber, C. Wöhrmann, R. Wolf

Institute of Nuclear and Particle Physics (INPP), NCSR Demokritos, Aghia Paraskevi, Greece
G. Anagnostou, P. Asenov, G. Daskalakis, T. Geralis, A. Kyriakis, D. Loukas, G. Paspalaki

National and Kapodistrian University of Athens, Athens, Greece
M. Diamantopoulou, G. Karathanasis, P. Kontaxakis, A. Manousakis-katsikakis, A. Panagiotou, I. Papavergou, N. Saoulidou, A. Stakia, K. Theofilatos, K. Vellidis, E. Vourliotis

National Technical University of Athens, Athens, Greece
G. Bakas, K. Kousouris, I. Papakrivopoulos, G. Tsipolitis

University of Ioánnina, Ioánnina, Greece
I. Evangelou, C. Foudas, P. Gianneios, P. Katsoulis, P. Kokkas, S. Mallios, K. Manitara, N. Manthos, I. Papadopoulos, J. Strologas, F. A. Triantis, D. Tsitsonis

MTA-ELTE Lendület CMS Particle and Nuclear Physics Group, Eötvös Loránd University, Budapest, Hungary
M. Bartók[20], M. Csanad, P. Major, K. Mandal, A. Mehta, M. I. Nagy, G. Pasztor, O. Surányi, G. I. Veres

Wigner Research Centre for Physics, Budapest, Hungary
G. Bencze, C. Hajdu, D. Horvath[21], F. Sikler, T. Vámi, V. Veszpremi, G. Vesztergombi[†]

Institute of Nuclear Research ATOMKI, Debrecen, Hungary
N. Beni, S. Czellar, J. Karancsi[20], A. Makovec, J. Molnar, Z. Szillasi

Institute of Physics, University of Debrecen, Debrecen, Hungary
P. Raics, D. Teyssier, Z. L. Trocsanyi, B. Ujvari

Eszterhazy Karoly University, Karoly Robert Campus, Gyongyos, Hungary
T. Csorgo, W. J. Metzger, F. Nemes, T. Novak

Indian Institute of Science (IISc), Bangalore, India
S. Choudhury, J. R. Komaragiri, P. C. Tiwari

National Institute of Science Education and Research, HBNI, Bhubaneswar, India
S. Bahinipati[23], C. Kar, G. Kole, P. Mal, V. K. Muraleedharan Nair Bindhu, A. Nayak[24], D. K. Sahoo[23], S. K. Swain

Panjab University, Chandigarh, India
S. Bansal, S. B. Beri, V. Bhatnagar, S. Chauhan, R. Chawla, N. Dhingra, R. Gupta, A. Kaur, M. Kaur, S. Kaur, P. Kumari, M. Lohan, M. Meena, K. Sandeep, S. Sharma, J. B. Singh, A. K. Virdi

University of Delhi, Delhi, India
A. Bhardwaj, B. C. Choudhary, R. B. Garg, M. Gola, S. Keshri, Ashok Kumar, S. Malhotra, M. Naimuddin, P. Priyanka, K. Ranjan, Aashaq Shah, R. Sharma

Saha Institute of Nuclear Physics, HBNI, Kolkata, India
R. Bhardwaj[25], M. Bharti[25], R. Bhattacharya, S. Bhattacharya, U. Bhawandeep[25], D. Bhowmik, S. Dey, S. Dutta, S. Ghosh, M. Maity[26], K. Mondal, S. Nandan, A. Purohit, P. K. Rout, G. Saha, S. Sarkar, T. Sarkar[26], M. Sharan, B. Singh[25], S. Thakur[25]

Indian Institute of Technology Madras, Madras, India
P. K. Behera, P. Kalbhor, A. Muhammad, P. R. Pujahari, A. Sharma, A. K. Sikdar

Bhabha Atomic Research Centre, Mumbai, India
R. Chudasama, D. Dutta, V. Jha, V. Kumar, D. K. Mishra, P. K. Netrakanti, L. M. Pant, P. Shukla

Tata Institute of Fundamental Research-A, Mumbai, India
T. Aziz, M. A. Bhat, S. Dugad, G. B. Mohanty, N. Sur, RavindraKumar Verma

Tata Institute of Fundamental Research-B, Mumbai, India
S. Banerjee, S. Bhattacharya, S. Chatterjee, P. Das, M. Guchait, S. Karmakar, S. Kumar, G. Majumder, K. Mazumdar, N. Sahoo, S. Sawant

Indian Institute of Science Education and Research (IISER), Pune, India
S. Chauhan, S. Dube, V. Hegde, A. Kapoor, K. Kothekar, S. Pandey, A. Rane, A. Rastogi, S. Sharma

Institute for Research in Fundamental Sciences (IPM), Tehran, Iran
S. Chenarani[27], E. Eskandari Tadavani, S. M. Etesami[27], M. Khakzad, M. Mohammadi Najafabadi, M. Naseri, F. Rezaei Hosseinabadi

University College Dublin, Dublin, Ireland
M. Felcini, M. Grunewald

INFN Sezione di Bari[a], Università di Bari[b], Politecnico di Bari[c], Bari, Italy
M. Abbrescia[a,b], R. Aly[a,b,28], C. Calabria[a,b], A. Colaleo[a], D. Creanza[a,c], L. Cristella[a,b], N. De Filippis[a,c], M. De Palma[a,b], A. Di Florio[a,b], L. Fiore[a], A. Gelmi[a,b], G. Iaselli[a,c], M. Ince[a,b], S. Lezki[a,b], G. Maggi[a,c], M. Maggi[a], G. Miniello[a,b], S. My[a,b], S. Nuzzo[a,b], A. Pompili[a,b], G. Pugliese[a,c], R. Radogna[a], A. Ranieri[a], G. Selvaggi[a,b], L. Silvestris[a], R. Venditti[a], P. Verwilligen[a]

INFN Sezione di Bologna[a], Università di Bologna[b], Bologna, Italy
G. Abbiendi[a], C. Battilana[a,b], D. Bonacorsi[a,b], L. Borgonovi[a,b], S. Braibant-Giacomelli[a,b], R. Campanini[a,b], P. Capiluppi[a,b], A. Castro[a,b], F. R. Cavallo[a], C. Ciocca[a], G. Codispoti[a,b], M. Cuffiani[a,b], G. M. Dallavalle[a], F. Fabbri[a], A. Fanfani[a,b], E. Fontanesi, P. Giacomelli[a], C. Grandi[a], L. Guiducci[a,b], F. Iemmi[a,b], S. Lo Meo[a,29], S. Marcellini[a], G. Masetti[a], F. L. Navarria[a,b], A. Perrotta[a], F. Primavera[a,b], A. M. Rossi[a,b], T. Rovelli[a,b], G. P. Siroli[a,b], N. Tosi[a]

INFN Sezione di Catania[a], Università di Catania[b], Catania, Italy
S. Albergo[a,b,30], S. Costa[a,b], A. Di Mattia[a], R. Potenza[a,b], A. Tricomi[a,b,30], C. Tuve[a,b]

INFN Sezione di Firenze[a], Università di Firenze[b], Firenze, Italy
G. Barbagli[a], R. Ceccarelli, K. Chatterjee[a,b], V. Ciulli[a,b], C. Civinini[a], R. D'Alessandro[a,b], E. Focardi[a,b], G. Latino, P. Lenzi[a,b], M. Meschini[a], S. Paoletti[a], G. Sguazzoni[a], D. Strom[a], L. Viliani[a]

INFN Laboratori Nazionali di Frascati, Frascati, Italy
L. Benussi, S. Bianco, D. Piccolo

INFN Sezione di Genova[a], Università di Genova[b], Genova, Italy
M. Bozzo[a,b], F. Ferro[a], R. Mulargia[a,b], E. Robutti[a], S. Tosi[a,b]

INFN Sezione di Milano-Bicocca[a], Università di Milano-Bicocca[b], Milan, Italy
A. Benaglia[a], A. Beschi[a,b], F. Brivio[a,b], V. Ciriolo[a,b,16], S. Di Guida[a,b,16], M. E. Dinardo[a,b], P. Dini[a], S. Gennai[a], A. Ghezzi[a,b], P. Govoni[a,b], L. Guzzi[a,b], M. Malberti[a], S. Malvezzi[a], D. Menasce[a], F. Monti[a,b], L. Moroni[a], G. Ortona[a,b], M. Paganoni[a,b], D. Pedrini[a], S. Ragazzi[a,b], T. Tabarelli de Fatis[a,b], D. Zuolo[a,b]

INFN Sezione di Napoli[a], Università di Napoli 'Federico II' [b], Napoli, Italy, Università della Basilicata[c], Potenza, Italy, Università G. Marconi[d], Rome, Italy
S. Buontempo[a], N. Cavallo[a,c], A. De Iorio[a,b], A. Di Crescenzo[a,b], F. Fabozzi[a,c], F. Fienga[a], G. Galati[a], A. O. M. Iorio[a,b], L. Lista[a,b], S. Meola[a,d,16], P. Paolucci[a,16], B. Rossi[a], C. Sciacca[a,b], E. Voevodina[a,b]

INFN Sezione di Padova[a], Università di Padova[b], Padua, Italy, Università di Trento[c], Trento, Italy
P. Azzi[a], N. Bacchetta[a], D. D.Bisello[a,b], A. Boletti[a,b], A. Bragagnolo, R. Carlin[a,b], P. Checchia[a], P. De Castro Manzano[a], T. Dorigo[a], U. Dosselli[a], F. Gasparini[a,b], U. Gasparini[a,b], A. Gozzelino[a], S. Y. Hoh, P. Lujan, M. Margoni[a,b], A. T. Meneguzzo[a,b], J. Pazzini[a,b], M. Presilla[b], P. Ronchese[a,b], R. Rossin[a,b], F. Simonetto[a,b], A. Tiko, M. Tosi[a,b], M. Zanetti[a,b], P. Zotto[a,b], G. Zumerle[a,b]

INFN Sezione di Pavia[a], Università di Pavia[b], Pavia, Italy
A. Braghieri[a], P. Montagna[a,b], S. P. Ratti[a,b], V. Re[a], M. Ressegotti[a,b], C. Riccardi[a,b], P. Salvini[a], I. Vai[a,b], P. Vitulo[a,b]

INFN Sezione di Perugia[a], Università di Perugia[b], Perugia, Italy
M. Biasini[a,b], G. M. Bilei[a], C. Cecchi[a,b], D. Ciangottini[a,b], L. Fanò[a,b], P. Lariccia[a,b], R. Leonardi[a,b], E. Manoni[a], G. Mantovani[a,b], V. Mariani[a,b], M. Menichelli[a], A. Rossi[a,b], A. Santocchia[a,b], D. Spiga[a]

INFN Sezione di Pisa[a], Università di Pisa[b], Scuola Normale Superiore di Pisa[c], Pisa, Italy
K. Androsov[a], P. Azzurri[a], G. Bagliesi[a], V. Bertacchi[a,c], L. Bianchini[a], T. Boccali[a], R. Castaldi[a], M. A. Ciocci[a,b], R. Dell'Orso[a], G. Fedi[a], L. Giannini[a,c], A. Giassi[a], M. T. Grippo[a], F. Ligabue[a,c], E. Manca[a,c], G. Mandorli[a,c], A. Messineo[a,b], F. Palla[a], A. Rizzi[a,b], G. Rolandi[31], S. Roy Chowdhury, A. Scribano[a], P. Spagnolo[a], R. Tenchini[a], G. Tonelli[a,b], N. Turini, A. Venturi[a], P. G. Verdini[a]

INFN Sezione di Roma[a], Sapienza Università di Roma[b], Rome, Italy
F. Cavallari[a], M. Cipriani[a,b], D. Del Re[a,b], E. Di Marco[a,b], M. Diemoz[a], E. Longo[a,b], B. Marzocchi[a,b], P. Meridiani[a], G. Organtini[a,b], F. Pandolfi[a], R. Paramatti[a,b], C. Quaranta[a,b], S. Rahatlou[a,b], C. Rovelli[a], F. Santanastasio[a,b], L. Soffi[a,b]

INFN Sezione di Torino[a], Università di Torino[b], Torino, Italy, Università del Piemonte Orientale[c], Novara, Italy
N. Amapane[a,b], R. Arcidiacono[a,c], S. Argiro[a,b], M. Arneodo[a,c], N. Bartosik[a], R. Bellan[a,b], C. Biino[a], A. Cappati[a,b], N. Cartiglia[a], S. Cometti[a], M. Costa[a,b], R. Covarelli[a,b], N. Demaria[a], B. Kiani[a,b], C. Mariotti[a], S. Maselli[a], E. Migliore[a,b], V. Monaco[a,b], E. Monteil[a,b], M. Monteno[a], M. M. Obertino[a,b], L. Pacher[a,b], N. Pastrone[a], M. Pelliccioni[a], G. L. Pinna Angioni[a,b], A. Romero[a,b], M. Ruspa[a,c], R. Sacchi[a,c], R. Salvatico[a,b], V. Sola[a], A. Solano[a,b], D. Soldi[a,b], A. Staiano[a]

INFN Sezione di Trieste[a], Università di Trieste[b], Trieste, Italy
S. Belforte[a], V. Candelise[a,b], M. Casarsa[a], F. Cossutti[a], A. Da Rold[a,b], G. Della Ricca[a,b], F. Vazzoler[a,b], A. Zanetti[a]

Kyungpook National University, Daegu, Korea
B. Kim, D. H. Kim, G. N. Kim, M. S. Kim, J. Lee, S. W. Lee, C. S. Moon, Y. D. Oh, S. I. Pak, S. Sekmen, D. C. Son, Y. C. Yang

Chonnam National University, Institute for Universe and Elementary Particles, Kwangju, Korea
H. Kim, D. H. Moon, G. Oh

Hanyang University, Seoul, Korea
B. Francois, T. J. Kim, J. Park

Korea University, Seoul, Korea
S. Cho, S. Choi, Y. Go, D. Gyun, S. Ha, B. Hong, K. Lee, K. S. Lee, J. Lim, J. Park, S. K. Park, Y. Roh, J. Yoo

Department of Physics, Kyung Hee University, Seoul, South Korea
J. Goh

Sejong University, Seoul, Korea
H. S. Kim

Seoul National University, Seoul, Korea
J. Almond, J. H. Bhyun, J. Choi, S. Jeon, J. Kim, J. S. Kim, H. Lee, K. Lee, S. Lee, K. Nam, M. Oh, S. B. Oh, B. C. Radburn-Smith, U. K. Yang, H. D. Yoo, I. Yoon, G. B. Yu

University of Seoul, Seoul, Korea
D. Jeon, H. Kim, J. H. Kim, J. S. H. Lee, I. C. Park, I. Watson

Sungkyunkwan University, Suwon, Korea
Y. Choi, C. Hwang, Y. Jeong, J. Lee, Y. Lee, I. Yu

Riga Technical University, Riga, Latvia
V. Veckalns[32]

Vilnius University, Vilnius, Lithuania
V. Dudenas, A. Juodagalvis, G. Tamulaitis, J. Vaitkus

National Centre for Particle Physics, Universiti Malaya, Kuala Lumpur, Malaysia
Z. A. Ibrahim, F. Mohamad Idris[33], W. A. T. Wan Abdullah, M. N. Yusli, Z. Zolkapli

Universidad de Sonora (UNISON), Hermosillo, Mexico
J. F. Benitez, A. Castaneda Hernandez, J. A. Murillo Quijada, L. Valencia Palomo

Centro de Investigacion y de Estudios Avanzados del IPN, Mexico City, Mexico
H. Castilla-Valdez, E. De La Cruz-Burelo, I. Heredia-De La Cruz[34], R. Lopez-Fernandez, A. Sanchez-Hernandez

Universidad Iberoamericana, Mexico City, Mexico
S. Carrillo Moreno, C. Oropeza Barrera, M. Ramirez-Garcia, F. Vazquez Valencia

Benemerita Universidad Autonoma de Puebla, Puebla, Mexico
J. Eysermans, I. Pedraza, H. A. Salazar Ibarguen, C. Uribe Estrada

Universidad Autónoma de San Luis Potosí, San Luis Potosí, Mexico
A. Morelos Pineda

University of Montenegro, Podgorica, Montenegro
N. Raicevic

University of Auckland, Auckland, New Zealand
D. Krofcheck

University of Canterbury, Christchurch, New Zealand
S. Bheesette, P. H. Butler

National Centre for Physics, Quaid-I-Azam University, Islamabad, Pakistan
A. Ahmad, M. Ahmad, Q. Hassan, H. R. Hoorani, W. A. Khan, M. A. Shah, M. Shoaib, M. Waqas

AGH University of Science and Technology Faculty of Computer Science, Electronics and Telecommunications, Krakow, Poland
V. Avati, L. Grzanka, M. Malawski

National Centre for Nuclear Research, Swierk, Poland
H. Bialkowska, M. Bluj, B. Boimska, M. Górski, M. Kazana, M. Szleper, P. Zalewski

Institute of Experimental Physics, Faculty of Physics, University of Warsaw, Warsaw, Poland
K. Bunkowski, A. Byszuk[35], K. Doroba, A. Kalinowski, M. Konecki, J. Krolikowski, M. Misiura, M. Olszewski, A. Pyskir, M. Walczak

Laboratório de Instrumentação e Física Experimental de Partículas, Lisboa, Portugal
M. Araujo, P. Bargassa, D. Bastos, A. Di Francesco, P. Faccioli, B. Galinhas, M. Gallinaro, J. Hollar, N. Leonardo, J. Seixas, K. Shchelina, G. Strong, O. Toldaiev, J. Varela

Joint Institute for Nuclear Research, Dubna, Russia
V. Alexakhin, A. Baginyan, M. Gavrilenko, I. Golutvin, I. Gorbunov, A. Kamenev, V. Karjavine, V. Korenkov, A. Lanev, A. Malakhov, V. Matveev[36,37], V. V. Mitsyn, P. Moisenz, V. Palichik, V. Perelygin, M. Savina, S. Shmatov, S. Shulha, V. Trofimov, A. Zarubin

Petersburg Nuclear Physics Institute, Gatchina (St. Petersburg), Russia
L. Chtchipounov, V. Golovtsov, Y. Ivanov, V. Kim[38], E. Kuznetsova[39], P. Levchenko, V. Murzin, V. Oreshkin, I. Smirnov, D. Sosnov, V. Sulimov, L. Uvarov, A. Vorobyev

Institute for Nuclear Research, Moscow, Russia
Yu. Andreev, A. Dermenev, S. Gninenko, N. Golubev, A. Karneyeu, M. Kirsanov, N. Krasnikov, A. Pashenkov, D. Tlisov, A. Toropin

Institute for Theoretical and Experimental Physics named by A.I. Alikhanov of NRC 'Kurchatov Institute', Moscow, Russia
V. Epshteyn, V. Gavrilov, N. Lychkovskaya, A. Nikitenko[40], V. Popov, I. Pozdnyakov, G. Safronov, A. Spiridonov, A. Stepennov, M. Toms, E. Vlasov, A. Zhokin

Moscow Institute of Physics and Technology, Moscow, Russia
T. Aushev

National Research Nuclear University 'Moscow Engineering Physics Institute' (MEPhI), Moscow, Russia
M. Chadeeva[41], P. Parygin, D. Philippov, E. Popova, V. Rusinov

P.N. Lebedev Physical Institute, Moscow, Russia
V. Andreev, M. Azarkin, I. Dremin, M. Kirakosyan, A. Terkulov

Skobeltsyn Institute of Nuclear Physics, Lomonosov Moscow State University, Moscow, Russia
A. Baskakov, A. Belyaev, E. Boos, V. Bunichev, M. Dubinin[42], L. Dudko, A. Ershov, A. Gribushin, V. Klyukhin, O. Kodolova, I. Lokhtin, S. Obraztsov, V. Savrin

Novosibirsk State University (NSU), Novosibirsk, Russia
A. Barnyakov[43], V. Blinov[43], T. Dimova[43], L. Kardapoltsev[43], Y. Skovpen[43]

Institute for High Energy Physics of National Research Centre 'Kurchatov Institute', Protvino, Russia
I. Azhgirey, I. Bayshev, S. Bitioukov, V. Kachanov, D. Konstantinov, P. Mandrik, V. Petrov, R. Ryutin, S. Slabospitskii, A. Sobol, S. Troshin, N. Tyurin, A. Uzunian, A. Volkov

National Research Tomsk Polytechnic University, Tomsk, Russia
A. Babaev, A. Iuzhakov, V. Okhotnikov

Tomsk State University, Tomsk, Russia
V. Borchsh, V. Ivanchenko, E. Tcherniaev

University of Belgrade: Faculty of Physics and VINCA Institute of Nuclear Sciences, Belgrade, Serbia
P. Adzic[44], P. Cirkovic, D. Devetak, M. Dordevic, P. Milenovic, J. Milosevic, M. Stojanovic

Centro de Investigaciones Energéticas Medioambientales y Tecnológicas (CIEMAT), Madrid, Spain
M. Aguilar-Benitez, J. Alcaraz Maestre, A. lvarez Fernández, I. Bachiller, M. Barrio Luna, J. A. Brochero Cifuentes, C. A. Carrillo Montoya, M. Cepeda, M. Cerrada, N. Colino, B. De La Cruz, A. Delgado Peris, C. Fernandez Bedoya, J. P. Fernández Ramos, J. Flix, M. C. Fouz, O. Gonzalez Lopez, S. Goy Lopez, J. M. Hernandez, M. I. Josa, D. Moran, Navarro Tobar, A. Pérez-Calero Yzquierdo, J. Puerta Pelayo, I. Redondo, L. Romero, S. Sánchez Navas, M. S. Soares, A. Triossi, C. Willmott

Universidad Autónoma de Madrid, Madrid, Spain
C. Albajar, J. F. de Trocóniz

Universidad de Oviedo, Instituto Universitario de Ciencias y Tecnologías Espaciales de Asturias (ICTEA), Oviedo, Spain
B. Alvarez Gonzalez, J. Cuevas, C. Erice, J. Fernandez Menendez, S. Folgueras, I. Gonzalez Caballero, J. R. González Fernández, E. Palencia Cortezon, V. Rodríguez Bouza, S. Sanchez Cruz

Instituto de Física de Cantabria (IFCA), CSIC-Universidad de Cantabria, Santander, Spain
I. J. Cabrillo, A. Calderon, B. Chazin Quero, J. Duarte Campderros, M. Fernandez, P. J. Fernández Manteca, A. García Alonso, G. Gomez, C. Martinez Rivero, P. Martinez Ruiz del Arbol, F. Matorras, J. Piedra Gomez, C. Prieels, T. Rodrigo, A. Ruiz-Jimeno, L. Russo[45], L. Scodellaro, N. Trevisani, I. Vila, J. M. Vizan Garcia

University of Colombo, Colombo, Sri Lanka
K. Malagalage

Department of Physics, University of Ruhuna, Matara, Sri Lanka
W. G. D. Dharmaratna, N. Wickramage

CERN, European Organization for Nuclear Research, Geneva, Switzerland
D. Abbaneo, B. Akgun, E. Auffray, G. Auzinger, J. Baechler, P. Baillon, A. H. Ball, D. Barney, J. Bendavid, M. Bianco, A. Bocci, P. Bortignon, E. Bossini, C. Botta, E. Brondolin, T. Camporesi, A. Caratelli, G. Cerminara, E. Chapon, G. Cucciati, D. d'Enterria, A. Dabrowski, N. Daci, V. Daponte, A. David, O. Davignon, A. De Roeck, N. Deelen, M. Deile, M. Dobson, M. Dünser, N. Dupont, A. Elliott-Peisert, F. Fallavollita[46], D. Fasanella, S. Fiorendi, G. Franzoni, J. Fulcher, W. Funk, S. Giani, D. Gigi, A. Gilbert, K. Gill, F. Glege, M. Gruchala, M. Guilbaud, D. Gulhan, J. Hegeman, C. Heidegger, Y. Iiyama, V. Innocente, P. Janot, O. Karacheban[19], J. Kaspar, J. Kieseler, M. Krammer[1], C. Lange, P. Lecoq, C. Lourenço, L. Malgeri, M. Mannelli, A. Massironi, F. Meijers, J. A. Merlin, S. Mersi, E. Meschi, F. Moortgat, M. Mulders, J. Ngadiuba, S. Nourbakhsh, S. Orfanelli, L. Orsini, F. Pantaleo[16], L. Pape, E. Perez, M. Peruzzi, A. Petrilli, G. Petrucciani, A. Pfeiffer, M. Pierini, F. M. Pitters, D. Rabady, A. Racz, M. Rovere, H. Sakulin, C. Schäfer, C. Schwick, M. Selvaggi, A. Sharma, P. Silva, W. Snoeys, P. Sphicas[47], J. Steggemann, S. Summers, V. R. Tavolaro, D. Treille, A. Tsirou, A. Vartak, M. Verzetti, W. D. Zeuner

Paul Scherrer Institut, Villigen, Switzerland
L. Caminada[48], K. Deiters, W. Erdmann, R. Horisberger, Q. Ingram, H. C. Kaestli, D. Kotlinski, U. Langenegger, T. Rohe, S. A. Wiederkehr

ETH Zurich-Institute for Particle Physics and Astrophysics (IPA), Zurich, Switzerland
M. Backhaus, P. Berger, N. Chernyavskaya, G. Dissertori, M. Dittmar, M. Donegà, C. Dorfer, T. A. Gómez Espinosa, C. Grab, D. Hits, T. Klijnsma, W. Lustermann, R. A. Manzoni, M. Marionneau, M. T. Meinhard, F. Micheli, P. Musella, F. Nessi-Tedaldi, F. Pauss, G. Perrin, L. Perrozzi, S. Pigazzini, M. G. Ratti, M. Reichmann, C. Reissel, T. Reitenspiess, D. Ruini, D. A. Sanz Becerra, M. Schönenberger, L. Shchutska, M. L. Vesterbacka Olsson, R. Wallny, D. H. Zhu

Universität Zürich, Zurich, Switzerland
T. K. Aarrestad, C. Amsler[49], D. Brzhechko, M. F. Canelli, A. De Cosa, R. Del Burgo, S. Donato, B. Kilminster, S. Leontsinis, V. M. Mikuni, I. Neutelings, G. Rauco, P. Robmann, D. Salerno, K. Schweiger, C. Seitz, Y. Takahashi, S. Wertz, A. Zucchetta

National Central University, Chung-Li, Taiwan
T. H. Doan, C. M. Kuo, W. Lin, A. Roy, S. S. Yu

National Taiwan University (NTU), Taipei, Taiwan
P. Chang, Y. Chao, K. F. Chen, P. H. Chen, W.-S. Hou, Y. y. Li, R.-S. Lu, E. Paganis, A. Psallidas, A. Steen

Chulalongkorn University, Faculty of Science, Department of Physics, Bangkok, Thailand
B. Asavapibhop, C. Asawatangtrakuldee, N. Srimanobhas, N. Suwonjandee

ukurova University, Physics Department, Science and Art Faculty, Adana, Turkey
A. Bat, F. Boran, S. Cerci[50], S. Damarseckin[51], Z. S. Demiroglu, F. Dolek, C. Dozen, I. Dumanoglu, G. Gokbulut, EmineGurpinar Guler[52], Y. Guler, I. Hos[53], C. Isik, E. E. Kangal[54], O. Kara, A. Kayis Topaksu, U. Kiminsu, M. Oglakci, G. Onengut, K. Ozdemir[55], S. Ozturk[56], A. E. Simsek, D. Sunar Cerci[50], U. G. Tok, S. Turkcapar, I. S. Zorbakir, C. Zorbilmez

Middle East Technical University, Physics Department, Ankara, Turkey
B. Isildak[57], G. Karapinar[58], M. Yalvac

Bogazici University, Istanbul, Turkey
I. O. Atakisi, E. Gülmez, M. Kaya[59], O. Kaya[60], B. Kaynak, Ö. Özçelik, S. Tekten, E. A. Yetkin[61]

Istanbul Technical University, Istanbul, Turkey
A. Cakir, K. Cankocak, Y. Komurcu, S. Sen[62]

Istanbul University, Istanbul, Turkey
S. Ozkorucuklu

Institute for Scintillation Materials of National Academy of Science of Ukraine, Kharkov, Ukraine
B. Grynyov

National Scientific Center, Kharkov Institute of Physics and Technology, Kharkov, Ukraine
L. Levchuk

University of Bristol, Bristol, UK
F. Ball, E. Bhal, S. Bologna, J. J. Brooke, D. Burns[63], E. Clement, D. Cussans, H. Flacher, J. Goldstein, G. P. Heath, H. F. Heath, L. Kreczko, S. Paramesvaran, B. Penning, T. Sakuma, S. Seif El Nasr-Storey, D. Smith[63], V. J. Smith, J. Taylor, A. Titterton

Rutherford Appleton Laboratory, Didcot, UK
K. W. Bell, A. Belyaev[64], C. Brew, R. M. Brown, D. Cieri, D. J. A. Cockerill, J. A. Coughlan, K. Harder, S. Harper, J. Linacre, K. Manolopoulos, D. M. Newbold, E. Olaiya, D. Petyt, T. Reis, T. Schuh, C. H. Shepherd-Themistocleous, A. Thea, I. R. Tomalin, T. Williams, W. J. Womersley

Imperial College, London, UK
R. Bainbridge, P. Bloch, J. Borg, S. Breeze, O. Buchmuller, A. Bundock, GurpreetSingh CHAHAL[65], D. Colling, P. Dauncey, G. Davies, M. Della Negra, R. Di Maria, P. Everaerts, G. Hall, G. Iles, T. James, M. Komm, C. Laner, L. Lyons, A.-M. Magnan, S. Malik, A. Martelli, V. Milosevic, J. Nash[66], V. Palladino, M. Pesaresi, D. M. Raymond, A. Richards, A. Rose, E. Scott, C. Seez, A. Shtipliyski, M. Stoye, T. Strebler, A. Tapper, K. Uchida, T. Virdee[16], N. Wardle, D. Winterbottom, J. Wright, A. G. Zecchinelli, S. C. Zenz

Brunel University, Uxbridge, UK
J. E. Cole, P. R. Hobson, A. Khan, P. Kyberd, C. K. Mackay, A. Morton, I. D. Reid, L. Teodorescu, S. Zahid

Baylor University, Waco, USA
K. Call, J. Dittmann, K. Hatakeyama, C. Madrid, B. McMaster, N. Pastika, C. Smith

Catholic University of America, Washington DC, USA
R. Bartek, A. Dominguez, R. Uniyal

The University of Alabama, Tuscaloosa, USA
A. Buccilli, S. I. Cooper, C. Henderson, P. Rumerio, C. West

Boston University, Boston, USA
D. Arcaro, T. Bose, Z. Demiragli, D. Gastler, S. Girgis, D. Pinna, C. Richardson, J. Rohlf, D. Sperka, I. Suarez, L. Sulak, D. Zou

Brown University, Providence, USA
G. Benelli, B. Burkle, X. Coubez, D. Cutts, Y. t. Duh, M. Hadley, J. Hakala, U. Heintz, J. M. Hogan[67], K. H. M. Kwok, E. Laird, G. Landsberg, J. Lee, Z. Mao, M. Narain, S. Sagir[68], R. Syarif, E. Usai, D. Yu

University of California, Davis, Davis, USA
R. Band, C. Brainerd, R. Breedon, M. Calderon De La Barca Sanchez, M. Chertok, J. Conway, R. Conway, P. T. Cox, R. Erbacher, C. Flores, G. Funk, F. Jensen, W. Ko, O. Kukral, R. Lander, M. Mulhearn, D. Pellett, J. Pilot, M. Shi, D. Taylor, K. Tos, M. Tripathi, Z. Wang, F. Zhang

University of California, Los Angeles, USA
M. Bachtis, C. Bravo, R. Cousins, A. Dasgupta, A. Florent, J. Hauser, M. Ignatenko, N. Mccoll, W. A. Nash, S. Regnard, D. Saltzberg, C. Schnaible, B. Stone, V. Valuev

University of California, Riverside, Riverside, USA
K. Burt, R. Clare, J. W. Gary, S. M. A. Ghiasi Shirazi, G. Hanson, G. Karapostoli, E. Kennedy, O. R. Long, M. Olmedo Negrete, M. I. Paneva, W. Si, L. Wang, H. Wei, S. Wimpenny, B. R. Yates, Y. Zhang

University of California, San Diego, La Jolla, USA
J. G. Branson, P. Chang, S. Cittolin, M. Derdzinski, R. Gerosa, D. Gilbert, B. Hashemi, D. Klein, V. Krutelyov, J. Letts, M. Masciovecchio, S. May, S. Padhi, M. Pieri, V. Sharma, M. Tadel, F. Würthwein, A. Yagil, G. Zevi Della Porta

University of California, Santa Barbara-Department of Physics, Santa Barbara, USA
N. Amin, R. Bhandari, C. Campagnari, M. Citron, O. Colegrove, V. Dutta, M. Franco Sevilla, L. Gouskos, J. Incandela, B. Marsh, H. Mei, A. Ovcharova, H. Qu, J. Richman, U. Sarica, D. Stuart, S. Wang

California Institute of Technology, Pasadena, USA
D. Anderson, A. Bornheim, O. Cerri, I. Dutta, J. M. Lawhorn, N. Lu, J. Mao, H. B. Newman, T. Q. Nguyen, J. Pata, M. Spiropulu, J. R. Vlimant, S. Xie, Z. Zhang, R. Y. Zhu

Carnegie Mellon University, Pittsburgh, USA
M. B. Andrews, T. Ferguson, T. Mudholkar, M. Paulini, M. Sun, I. Vorobiev, M. Weinberg

University of Colorado Boulder, Boulder, USA
J. P. Cumalat, W. T. Ford, A. Johnson, E. MacDonald, T. Mulholland, R. Patel, A. Perloff, K. Stenson, K. A. Ulmer, S. R. Wagner

Cornell University, Ithaca, USA
J. Alexander, J. Chaves, Y. Cheng, J. Chu, A. Datta, A. Frankenthal, K. Mcdermott, J. R. Patterson, D. Quach, A. Rinkevicius[69], A. Ryd, S. M. Tan, Z. Tao, J. Thom, P. Wittich, M. Zientek

Fermi National Accelerator Laboratory, Batavia, USA
S. Abdullin, M. Albrow, M. Alyari, G. Apollinari, A. Apresyan, A. Apyan, S. Banerjee, L. A. T. Bauerdick, A. Beretvas, J. Berryhill, P. C. Bhat, K. Burkett, J. N. Butler, A. Canepa, G. B. Cerati, H. W. K. Cheung, F. Chlebana, M. Cremonesi, J. Duarte, V. D. Elvira, J. Freeman, Z. Gecse, E. Gottschalk, L. Gray, D. Green, S. Grünendahl, O. Gutsche, AllisonReinsvold Hall, J. Hanlon, R. M. Harris, S. Hasegawa, R. Heller, J. Hirschauer, B. Jayatilaka, S. Jindariani, M. Johnson, U. Joshi, B. Klima, M. J. Kortelainen, B. Kreis, S. Lammel, J. Lewis, D. Lincoln, R. Lipton, M. Liu, T. Liu, J. Lykken, K. Maeshima, J. M. Marraffino, D. Mason, P. McBride, P. Merkel, S. Mrenna, S. Nahn, V. O'Dell, V. Papadimitriou, K. Pedro, C. Pena, G. Rakness, F. Ravera, L. Ristori, B. Schneider, E. Sexton-Kennedy, N. Smith, A. Soha, W. J. Spalding, L. Spiegel, S. Stoynev, J. Strait, N. Strobbe, L. Taylor, S. Tkaczyk, N. V. Tran, L. Uplegger, E. W. Vaandering, C. Vernieri, M. Verzocchi, R. Vidal, M. Wang, H. A. Weber

University of Florida, Gainesville, USA
D. Acosta, P. Avery, D. Bourilkov, A. Brinkerhoff, L. Cadamuro, A. Carnes, V. Cherepanov, D. Curry, F. Errico, R. D. Field, S. V. Gleyzer, B. M. Joshi, M. Kim, J. Konigsberg, A. Korytov, K. H. Lo, P. Ma, K. Matchev, N. Menendez, G. Mitselmakher, D. Rosenzweig, K. Shi, J. Wang, S. Wang, X. Zuo

Florida International University, Miami, USA
Y. R. Joshi

Florida State University, Tallahassee, USA
T. Adams, A. Askew, S. Hagopian, V. Hagopian, K. F. Johnson, R. Khurana, T. Kolberg, G. Martinez, T. Perry, H. Prosper, C. Schiber, R. Yohay, J. Zhang

Florida Institute of Technology, Melbourne, USA
M. M. Baarmand, V. Bhopatkar, M. Hohlmann, D. Noonan, M. Rahmani, M. Saunders, F. Yumiceva

University of Illinois at Chicago (UIC), Chicago, USA
M. R. Adams, L. Apanasevich, D. Berry, R. R. Betts, R. Cavanaugh, X. Chen, S. Dittmer, O. Evdokimov, C. E. Gerber, D. A. Hangal, D. J. Hofman, K. Jung, C. Mills, T. Roy, M. B. Tonjes, N. Varelas, H. Wang, X. Wang, Z. Wu

The University of Iowa, Iowa City, USA
M. Alhusseini, B. Bilki[52], W. Clarida, K. Dilsiz[70], S. Durgut, R. P. Gandrajula, M. Haytmyradov, V. Khristenko, O. K. Köseyan, J.-P. Merlo, A. Mestvirishvili[71], A. Moeller, J. Nachtman, H. Ogul[72], Y. Onel, F. Ozok[73], A. Penzo, C. Snyder, E. Tiras, J. Wetzel

Johns Hopkins University, Baltimore, USA
B. Blumenfeld, A. Cocoros, N. Eminizer, D. Fehling, L. Feng, A. V. Gritsan, W. T. Hung, P. Maksimovic, J. Roskes, M. Swartz, M. Xiao

The University of Kansas, Lawrence, USA
C. Baldenegro Barrera, P. Baringer, A. Bean, S. Boren, J. Bowen, A. Bylinkin, T. Isidori, S. Khalil, J. King, G. Krintiras, A. Kropivnitskaya, C. Lindsey, D. Majumder, W. Mcbrayer, N. Minafra, M. Murray, C. Rogan, C. Royon, S. Sanders, E. Schmitz, J. D. Tapia Takaki, Q. Wang, J. Williams, G. Wilson

Kansas State University, Manhattan, USA
S. Duric, A. Ivanov, K. Kaadze, D. Kim, Y. Maravin, D. R. Mendis, T. Mitchell, A. Modak, A. Mohammadi

Lawrence Livermore National Laboratory, Livermore, USA
F. Rebassoo, D. Wright

University of Maryland, College Park, USA
A. Baden, O. Baron, A. Belloni, S. C. Eno, Y. Feng, N. J. Hadley, S. Jabeen, G. Y. Jeng, R. G. Kellogg, J. Kunkle, A. C. Mignerey, S. Nabili, F. Ricci-Tam, M. Seidel, Y. H. Shin, A. Skuja, S. C. Tonwar, K. Wong

Massachusetts Institute of Technology, Cambridge, USA
D. Abercrombie, B. Allen, A. Baty, R. Bi, S. Brandt, W. Busza, I. A. Cali, M. D'Alfonso, G. Gomez Ceballos, M. Goncharov, P. Harris, D. Hsu, M. Hu, M. Klute, D. Kovalskyi, Y.-J. Lee, P. D. Luckey, B. Maier, A. C. Marini, C. Mcginn, C. Mironov, S. Narayanan, X. Niu, C. Paus, D. Rankin, C. Roland, G. Roland, Z. Shi, G. S. F. Stephans, K. Sumorok, K. Tatar, D. Velicanu, J. Wang, T. W. Wang, B. Wyslouch

University of Minnesota, Minneapolis, USA
A. C. Benvenuti[†], R. M. Chatterjee, A. Evans, S. Guts, P. Hansen, J. Hiltbrand, Sh. Jain, Y. Kubota, Z. Lesko, J. Mans, R. Rusack, M. A. Wadud

University of Mississippi, Oxford, USA
J. G. Acosta, S. Oliveros

University of Nebraska-Lincoln, Lincoln, USA
K. Bloom, D. R. Claes, C. Fangmeier, L. Finco, F. Golf, R. Gonzalez Suarez, R. Kamalieddin, I. Kravchenko, J. E. Siado, G. R. Snow, B. Stieger

State University of New York at Buffalo, Buffalo, USA
G. Agarwal, C. Harrington, I. Iashvili, A. Kharchilava, C. McLean, D. Nguyen, A. Parker, J. Pekkanen, S. Rappoccio, B. Roozbahani

Northeastern University, Boston, USA
G. Alverson, E. Barberis, C. Freer, Y. Haddad, A. Hortiangtham, G. Madigan, D. M. Morse, T. Orimoto, L. Skinnari, A. Tishelman-Charny, T. Wamorkar, B. Wang, A. Wisecarver, D. Wood

Northwestern University, Evanston, USA
S. Bhattacharya, J. Bueghly, T. Gunter, K. A. Hahn, N. Odell, M. H. Schmitt, K. Sung, M. Trovato, M. Velasco

University of Notre Dame, Notre Dame, USA
R. Bucci, N. Dev, R. Goldouzian, M. Hildreth, K. Hurtado Anampa, C. Jessop, D. J. Karmgard, K. Lannon, W. Li, N. Loukas, N. Marinelli, I. Mcalister, F. Meng, C. Mueller, Y. Musienko[36], M. Planer, R. Ruchti, P. Siddireddy, G. Smith, S. Taroni, M. Wayne, A. Wightman, M. Wolf, A. Woodard

The Ohio State University, Columbus, USA
J. Alimena, B. Bylsma, L. S. Durkin, S. Flowers, B. Francis, C. Hill, W. Ji, A. Lefeld, T. Y. Ling, B. L. Winer

Princeton University, Princeton, USA
S. Cooperstein, G. Dezoort, P. Elmer, J. Hardenbrook, N. Haubrich, S. Higginbotham, A. Kalogeropoulos, S. Kwan, D. Lange, M. T. Lucchini, J. Luo, D. Marlow, K. Mei, I. Ojalvo, J. Olsen, C. Palmer, P. Piroué, J. Salfeld-Nebgen, D. Stickland, C. Tully, Z. Wang

University of Puerto Rico, Mayaguez, USA
S. Malik, S. Norberg

Purdue University, West Lafayette, USA
A. Barker, V. E. Barnes, S. Das, L. Gutay, M. Jones, A. W. Jung, A. Khatiwada, B. Mahakud, D. H. Miller, G. Negro, N. Neumeister, C. C. Peng, S. Piperov, H. Qiu, J. F. Schulte, J. Sun, F. Wang, R. Xiao, W. Xie

Purdue University Northwest, Hammond, USA
T. Cheng, J. Dolen, N. Parashar

Rice University, Houston, USA
K. M. Ecklund, S. Freed, F. J. M. Geurts, M. Kilpatrick, Arun Kumar, W. Li, B. P. Padley, R. Redjimi, J. Roberts, J. Rorie, W. Shi, A. G. Stahl Leiton, Z. Tu, A. Zhang

University of Rochester, Rochester, USA
A. Bodek, P. de Barbaro, R. Demina, J. L. Dulemba, C. Fallon, T. Ferbel, M. Galanti, A. Garcia-Bellido, J. Han, O. Hindrichs, A. Khukhunaishvili, E. Ranken, P. Tan, R. Taus

Rutgers, The State University of New Jersey, Piscataway, USA
B. Chiarito, J. P. Chou, A. Gandrakota, Y. Gershtein, E. Halkiadakis, A. Hart, M. Heindl, E. Hughes, S. Kaplan, S. Kyriacou, I. Laflotte, A. Lath, R. Montalvo, K. Nash, M. Osherson, H. Saka, S. Salur, S. Schnetzer, D. Sheffield, S. Somalwar, R. Stone, S. Thomas, P. Thomassen

University of Tennessee, Knoxville, USA
H. Acharya, A. G. Delannoy, G. Riley, S. Spanier

Texas A & M University, College Station, USA
O. Bouhali[74], A. Celik, M. Dalchenko, M. De Mattia, A. Delgado, S. Dildick, R. Eusebi, J. Gilmore, T. Huang, T. Kamon[75], S. Luo, D. Marley, R. Mueller, D. Overton, L. Perniè, D. Rathjens, A. Safonov

Texas Tech University, Lubbock, USA
N. Akchurin, J. Damgov, F. De Guio, S. Kunori, K. Lamichhane, S. W. Lee, T. Mengke, S. Muthumuni, T. Peltola, S. Undleeb, I. Volobouev, Z. Wang, A. Whitbeck

Vanderbilt University, Nashville, USA
S. Greene, A. Gurrola, R. Janjam, W. Johns, C. Maguire, A. Melo, H. Ni, K. Padeken, F. Romeo, P. Sheldon, S. Tuo, J. Velkovska, M. Verweij

University of Virginia, Charlottesville, USA
M. W. Arenton, P. Barria, B. Cox, G. Cummings, R. Hirosky, M. Joyce, A. Ledovskoy, C. Neu, B. Tannenwald, Y. Wang, E. Wolfe, F. Xia

Wayne State University, Detroit, USA
R. Harr, P. E. Karchin, N. Poudyal, J. Sturdy, P. Thapa, S. Zaleski

University of Wisconsin-Madison, Madison, WI, USA
J. Buchanan, C. Caillol, D. Carlsmith, S. Dasu, I. De Bruyn, L. Dodd, F. Fiori, C. Galloni, B. Gomber[76], H. He, M. Herndon, A. Hervé, U. Hussain, P. Klabbers, A. Lanaro, A. Loeliger, K. Long, R. Loveless, J. Madhusudanan Sreekala, T. Ruggles, A. Savin, V. Sharma, W. H. Smith, D. Teague, S. Trembath-reichert, N. Woods

† **Deceased**

1: Also at Vienna University of Technology, Vienna, Austria

2: Also at IRFU, CEA, Université Paris-Saclay, Gif-sur-Yvette, France
3: Also at Universidade Estadual de Campinas, Campinas, Brazil
4: Also at Federal University of Rio Grande do Sul, Porto Alegre, Brazil
5: Also at UFMS, Nova Andradina, Brazil
6: Also at Universidade Federal de Pelotas, Pelotas, Brazil
7: Also at Université Libre de Bruxelles, Bruxelles, Belgium
8: Also at University of Chinese Academy of Sciences, Beijing, China
9: Also at Institute for Theoretical and Experimental Physics named by A.I. Alikhanov of NRC 'Kurchatov Institute', Moscow, Russia
10: Also at Joint Institute for Nuclear Research, Dubna, Russia
11: Also at Ain Shams University, Cairo, Egypt
12: Also at Zewail City of Science and Technology, Zewail, Egypt
13: Also at Purdue University, West Lafayette, USA
14: Also at Université de Haute Alsace, Mulhouse, France
15: Also at Erzincan Binali Yildirim University,Erzincan,Turkey
16: Also at CERN, European Organization for Nuclear Research, Geneva, Switzerland
17: Also at RWTH Aachen University, III. Physikalisches Institut A, Aachen, Germany
18: Also at University of Hamburg, Hamburg, Germany
19: Also at Brandenburg University of Technology, Cottbus, Germany
20: Also at Institute of Physics, University of Debrecen, Debrecen, Hungary, Debrecen, Hungary
21: Also at Institute of Nuclear Research ATOMKI, Debrecen, Hungary
22: Also at MTA-ELTE Lendület CMS Particle and Nuclear Physics Group, Eötvös Loránd University, Budapest, Hungary, Budapest, Hungary
23: Also at IIT Bhubaneswar, Bhubaneswar, India, Bhubaneswar, India
24: Also at Institute of Physics, Bhubaneswar, India
25: Also at Shoolini University, Solan, India
26: Also at University of Visva-Bharati, Santiniketan, India
27: Also at Isfahan University of Technology, Isfahan, Iran
28: Now at INFN Sezione di Bari[a], Università di Bari[b], Politecnico di Bari[c], Bari, Italy
29: Also at Italian National Agency for New Technologies, Energy and Sustainable Economic Development, Bologna, Italy
30: Also at Centro Siciliano di Fisica Nucleare e di Struttura Della Materia, Catania, Italy
31: Also at Scuola Normale e Sezione dell'INFN, Pisa, Italy
32: Also at Riga Technical University, Riga, Latvia, Riga, Latvia
33: Also at Malaysian Nuclear Agency, MOSTI, Kajang, Malaysia
34: Also at Consejo Nacional de Ciencia y Tecnología, Mexico City, Mexico
35: Also at Warsaw University of Technology, Institute of Electronic Systems, Warsaw, Poland
36: Also at Institute for Nuclear Research, Moscow, Russia
37: Now at National Research Nuclear University 'Moscow Engineering Physics Institute' (MEPhI), Moscow, Russia
38: Also at St. Petersburg State Polytechnical University, St. Petersburg, Russia
39: Also at University of Florida, Gainesville, USA
40: Also at Imperial College, London, UK
41: Also at P.N. Lebedev Physical Institute, Moscow, Russia
42: Also at California Institute of Technology, Pasadena, USA
43: Also at Budker Institute of Nuclear Physics, Novosibirsk, Russia
44: Also at Faculty of Physics, University of Belgrade, Belgrade, Serbia
45: Also at Università degli Studi di Siena, Siena, Italy
46: Also at INFN Sezione di Pavia[a], Università di Pavia[b], Pavia, Italy, Pavia, Italy
47: Also at National and Kapodistrian University of Athens, Athens, Greece
48: Also at Universität Zürich, Zurich, Switzerland
49: Also at Stefan Meyer Institute for Subatomic Physics, Vienna, Austria, Vienna, Austria
50: Also at Adiyaman University, Adiyaman, Turkey
51: Also at Şırnak University, Sirnak, Turkey
52: Also at Beykent University, Istanbul, Turkey, Istanbul, Turkey

53: Also at Istanbul Aydin University, Istanbul, Turkey
54: Also at Mersin University, Mersin, Turkey
55: Also at Piri Reis University, Istanbul, Turkey
56: Also at Gaziosmanpasa University, Tokat, Turkey
57: Also at Ozyegin University, Istanbul, Turkey
58: Also at Izmir Institute of Technology, Izmir, Turkey
59: Also at Marmara University, Istanbul, Turkey
60: Also at Kafkas University, Kars, Turkey
61: Also at Istanbul Bilgi University, Istanbul, Turkey
62: Also at Hacettepe University, Ankara, Turkey
63: Also at Vrije Universiteit Brussel, Brussel, Belgium
64: Also at School of Physics and Astronomy, University of Southampton, Southampton, UK
65: Also at IPPP Durham University, Durham, UK
66: Also at Monash University, Faculty of Science, Clayton, Australia
67: Also at Bethel University, St. Paul, Minneapolis, USA, St. Paul, USA
68: Also at Karamanoğlu Mehmetbey University, Karaman, Turkey
69: Also at Vilnius University, Vilnius, Lithuania
70: Also at Bingol University, Bingol, Turkey
71: Also at Georgian Technical University, Tbilisi, Georgia
72: Also at Sinop University, Sinop, Turkey
73: Also at Mimar Sinan University, Istanbul, Istanbul, Turkey
74: Also at Texas A&M University at Qatar, Doha, Qatar
75: Also at Kyungpook National University, Daegu, Korea, Daegu, Korea
76: Also at University of Hyderabad, Hyderabad, India